



A Reflectron Time-of-Flight Mass Spectrometric Study on the Degradation Pathways of Glycine on Mars in the Presence of Perchlorates and Ionizing Radiation

Sándor Góbi^{1,2}, Marko Förstel^{1,2,3}, Pavlo Maksyutenko^{1,2}, and Ralf I. Kaiser^{1,2}

¹Department of Chemistry, University of Hawaii at Mānoa, Honolulu, HI 96822, USA; ralfk@hawaii.edu

²W.M. Keck Laboratory in Astrochemistry, University of Hawaii at Mānoa, Honolulu, HI 96822, USA

Received 2016 July 31; revised 2016 December 15; accepted 2016 December 19; published 2017 January 31

Abstract

The absence of abundant organics on the Martian surface is a much discussed observation. So far, no explanation is completely satisfactory. In this study we aim for a deeper understanding of the degradation processes of organics in the presence of perchlorates that can take place on the Martian surface. Our primary goal is to study the radiation-induced decomposition process of glycine ($\text{H}_2\text{NCH}_2\text{COOH}$) in the absence and presence of an oxidizer relevant to the Martian surface—perchlorate anions (ClO_4^-). Glycine and various samples of glycine- $1\text{-}^{13}\text{C}$ ($^+\text{H}_3\text{NCH}_2^{13}\text{COO}^-$)—magnesium perchlorate hexahydrate ($\text{Mg}(\text{ClO}_4)_2 \cdot 6\text{H}_2\text{O}$) were exposed to energetic electrons mimicking secondary electrons originating from the interaction of galactic cosmic rays (GCRs) with the Martian regolith. Using isotope-labeled and deuterated pure glycine samples such as glycine- $1\text{-}^{13}\text{C}$, glycine- d_5 ($^+\text{D}_3\text{NCD}_2\text{COO}^-$), glycine- N,N,N-d_3 ($^+\text{D}_3\text{NCH}_2\text{COO}^-$), and glycine- $2,2\text{-d}_2$ ($^+\text{H}_3\text{NCD}_2\text{COO}^-$), we can conclude that decarboxylation (carbon dioxide loss) of the glycine molecule is exclusively the first decay step during irradiation regardless of whether perchlorate anions are present or not. In pure glycine samples, the decarboxylation co-product methylamine (CH_3NH_2) and its radiolytic decay product ammonia could both be detected explicitly for the first time. In the presence of perchlorates, (partial) oxidation of the glycine decarboxylation product CH_3NH_2 may occur. Because the decarboxylation is an equilibrium reaction and the CH_3NH_2 is effectively removed from the system by this oxidation, glycine cannot be recycled. Therefore the depletion of the CH_3NH_2 facilitates the process, resulting in an overall 10-fold increase in the formation rate of carbon dioxide and its elevated concentrations in the perchlorate-containing irradiated samples.

Key words: astrochemistry – methods: laboratory: solid state – planets and satellites: surfaces – techniques: spectroscopic

1. Introduction

Revealing the reactions and degradation of organics on the Martian surface has been the focus of interest of the planetary science and astrobiology communities in recent decades. Basically, two main sources of organic compounds can be distinguished that allow for their accumulation on the surface of Mars: an in situ formation (ten Kate 2010) and an exogenous delivery via interplanetary dust particles (Flynn 1996; Moores & Schuerger 2012) and meteorites (Botta & Bada 2002), with the latter regarded as the predominant one. Once the organics are deposited on the surface, they are continuously exposed to solar photons, galactic cosmic rays (GCRs), and oxidizing agents such as perchlorates—inorganic compounds carrying the perchlorate anion (ClO_4^-). These cumulative effects can lead to their decomposition. Most importantly, the presence of oxidants in the Martian soil is the most widely accepted hypothesis for the scarcity of organics on the Martian surface. This was proposed based on the findings of the *Viking* (Biemann et al. 1976; Biemann & Bada 2011) and *Phoenix* landers (Sutter et al. 2009) and the lower-than-expected abundance of organics as revealed by the *Curiosity* rover (Freissinet et al. 2015).

Also, the effects of GCRs on the organics residing throughout the Martian subsurface pose important issues. Since Mars has only a very thin atmosphere at a level of 7 mbar of predominantly carbon dioxide (CO_2) (Armstrong et al. 2004) and has lacked a magnetic field over the past few billion years (Acuña et al. 1999), the Martian surface has been bombarded continuously by

energetic GCRs. Nonetheless, their effects are often neglected because their total energy flux is up to six orders of magnitude lower than that of solar photons. On average, GCRs deliver up to $10^4\text{--}10^5$ GeV $\text{m}^{-2} \text{s}^{-1}$ to the surface (Webber & Lezniak 1974; Molina-Cuberos et al. 2001; Dartnell et al. 2007) compared to about 5×10^{11} GeV $\text{m}^{-2} \text{s}^{-1}$ deposited by UV photons (Cockell & Raven 2004). However, solar photons are effectively absorbed within the first few monolayers of the solids (Muñoz-Caro et al. 2006), whereas energetic GCRs can penetrate up to several meters below the surface (Pavlov et al. 2012). This context makes GCRs the sole candidate for the destruction of organic compounds in deeper layers of Mars. Pavlov et al. (2012) calculated the dose that one organic molecule absorbs from GCRs to be about 0.045 Gy yr^{-1} ($3.5 \times 10^{-8} \text{ eV yr}^{-1}$ per glycine molecule). Although the effects of secondary oxidation processes from ionizing radiation on the mineral matrix were not included in these calculations, the calculated doses agreed nicely with the results of in situ measurements by the Radiation Assessment Detector instrument on the *Curiosity* rover (Hassler et al. 2014). Nevertheless, it should be highlighted that the work by Pavlov et al. (2012) takes only the degradation of ancient, indigenous organics into consideration, while neglecting their continuous resupply from meteorites and interplanetary dust particles. When the supply of organics via exogenous delivery (ten Kate et al. 2005) is compared to the destruction caused by cosmic rays, one has to conclude that the destruction is offset by the delivery of organics to the surface. A recent investigation likely confirms this assumption: pyrolysis experiments were carried out by the Sample Analysis at Mars instrument of the *Curiosity* rover and trace amounts of dichloroalkanes ($\text{C}_n\text{H}_{2n}\text{Cl}_2 < 70$ ppbw) and chlorobenzene ($\text{C}_6\text{H}_5\text{Cl}$, 150–300 ppbw) could be detected (Leshin

³ Present address: Technical University of Berlin, Department of Physics, Berlin, D-10623, Germany.

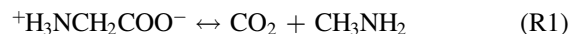
et al. 2013). These organics might be the products of the reaction between aliphatic and aromatic organics and perchlorates, both indigenous to the Martian soil (Freissinet et al. 2015, Miller et al. 2016).

In order to explain the results of the Mars landers and the lack of abundant organics, numerous laboratory experiments were performed examining the destruction of amino acids under simulated Martian condition. A compilation of these results can be found in Góbi et al. (2016a). Being the smallest building blocks of proteins and therefore essential for life, amino acids—especially the simplest representative glycine ($\text{H}_2\text{NCH}_2\text{COOH}$)—have been the focus of interest. Most of the works discuss UV irradiation and degradation (Oró & Holzer 1979; Stoker & Bullock 1997; Gerakines & Hudson 2015); the first experiment investigating the effects of GCRs was conducted just a decade ago. Besides high-energy γ -rays (Kminek & Bada 2006) and protons (ten Kate et al. 2005; Gerakines et al. 2012; Pilling et al. 2013), energetic electrons were also used to irradiate glycine samples under Martian-like conditions. These electron bombardments simulate the effect of secondary electrons formed in the track of GCRs once they penetrate solid matter such as minerals and organics within the Martian soil (Bennett et al. 2005; Bennett & Kaiser 2007). Therefore, various works in the past few years focused on the irradiation of glycine by energetic electrons (Maté et al. 2014, 2015; Pilling et al. 2014).

Despite the extensive research on the degradation of organics on Mars, an in situ analysis of the effects of neat perchlorates has emerged only recently. These experiments suggest that under Mars-relevant temperatures of 160–240 K, the decomposition rate of glycine effectively doubles in the presence of perchlorates upon exposure to energetic electrons (Góbi et al. 2016a). These perchlorates are abundant species throughout the solar system (Jackson et al. 2015). Based on the measurements made by the *Phoenix* lander (Hecht et al. 2009) and *Curiosity* rover (Glavin et al. 2013) perchlorates are thought to represent the most significant oxidants (Encrenaz et al. 2004, 2012) in the upper several centimeters in the Martian soil, with abundances as high as 1.0% by weight (Davila et al. 2013). They are assumed to be formed by heterogeneous photochemical (Smith et al. 2014) and photocatalytic (Carrier & Kounaves 2015) processes, or radiation-induced surface reactions within CO_2 ices (Kim et al. 2013; Wilson et al. 2016).

However, detailed mechanisms for the oxidation of organics in the presence of perchlorates were only partially unraveled. Experiments conducted by Góbi et al. (2016a) provided firm evidence that the glycine decomposition rates are twice as high in the presence of magnesium perchlorate hexahydrate ($\text{Mg}(\text{ClO}_4)_2 \cdot 6\text{H}_2\text{O}$); it is worth noting that magnesium perchlorate most likely occurs on Mars in its hydrated form (Chevrier et al. 2009; Toner et al. 2014). Since the destruction of perchlorates leads to atomic oxygen and eventually to molecular oxygen (Turner et al. 2016), this suggests that oxygen atoms—and possibly molecular oxygen—provide a unique oxidizing environment in the radiolyzed samples, thus accelerating the destruction of glycine. Furthermore, Góbi et al. (2016b) showed that the electron irradiation of perchlorates yields chlorine dioxide (ClO_2) besides oxygen, and this may act as an even more proficient oxidant that can also help the decomposition of organics on Mars. Hence, two simultaneous decay mechanisms should exist: the radiolytic degradation of glycine by high-energy electrons *and* the oxidation of glycine and/or its fragments by oxygen originating from the perchlorates (according to Turner

et al. 2016 the oxygen atoms originate exclusively from the irradiated perchlorate units, thus the crystalline water content does not take part in the process). Moreover, the formation rates of the glycine decarboxylation product CO_2 (reaction R1) and its radiolysis product carbon monoxide (CO , reaction R2) were also elevated by a factor of three to five. This also supported the aforementioned conclusion that an active oxygen-initiated chemistry represents the source of the accelerated rate constants of the decomposition of glycine.



A quantitative analysis of the CO_2 and CO products along with the degradation of glycine reveals that alternative degradation/oxidation products must exist. Here, three additional irradiation products were assigned tentatively by Fourier-transform infrared (FTIR) spectroscopy via band-broadening: methylamine (CH_3NH_2 , reaction R1) along with its decomposition products methane (CH_4 , reaction R3) and ammonia (NH_3 , reaction R4).



Since the concentration of these species is very low and their fundamentals mainly overlap with those of the parent molecule glycine, the previous study could not firmly identify those products based on infrared data. Therefore, alternative, more sensitive analytical methods are highly desired to search for the initial decomposition products of zwitterionic glycine (${}^+\text{H}_3\text{NCH}_2\text{COO}^-$) as well as for the products formed during the irradiation.

In our present work, we exploit state-of-the-art photoionization (PI) reflectron time-of-flight mass spectrometry (PI-ReTOF-MS) to detect the degradation *and* oxidation products of glycine in the presence of perchlorates as the products are released into the gas phase in the warm-up phase of the irradiated samples (Jones & Kaiser 2013; Maity et al. 2014; Abplanalp et al. 2016). Compared to traditional electron impact quadrupole mass spectrometry (EI-QMS), PI-ReTOF-MS has the unique advantage that fragmentation of the sublimed species after ionization can be neglected in almost all cases and only the parent molecular ions are observed. Additionally, it allows for discrimination of structural isomers of a particular molecule based on the different ionization energies of the isomers.

We further expose details of the destruction pathway and destruction kinetics of zwitterionic glycine. To do so we study the radiolytic decomposition of (partially) deuterated and ^{13}C -substituted reactants in form of glycine-1- ^{13}C (${}^+\text{H}_3\text{NCH}_2^{13}\text{COO}^-$), glycine- d_5 (${}^+\text{D}_3\text{NCD}_2\text{COO}^-$), glycine-N, N, N- d_3 (${}^+\text{D}_3\text{NCH}_2\text{COO}^-$), and glycine-2,2- d_2 (${}^+\text{H}_3\text{NCD}_2\text{COO}^-$) to ultimately trace the ^{13}C atom and extract the decomposition pathways of glycine in the presence of perchlorates on the Martian surface.

2. Experiment

The experiments were conducted in a contamination-free ultrahigh vacuum (UHV) stainless steel chamber, which can be evacuated to a base pressure of a few 10^{-11} mbar using oil-free magnetically suspended turbomolecular pumps and dry scroll backing pumps (Jones & Kaiser 2013; Maity et al. 2014; Abplanalp et al. 2016). A polished silver mirror is mounted on a cold finger made of oxygen-free high-conductivity copper using indium foil to ensure thermal conductivity. The cold finger is cooled by a closed-cycle helium refrigerator (Sumitomo Heavy

Industries, RDK-415E) and the temperature is set using a heater connected to a programmable temperature controller. The entire ensemble is freely rotatable within the horizontal center plane and translatable in the vertical axis via a UHV compatible bellows and a differentially pumped rotational feedthrough. The silver mirror acts as a substrate and was cooled down to 5.5 ± 0.1 K. We are aware that a temperature this low does not represent the Martian environment of 160–240 K. However, the present experiments are designed as a proof-of-concept study to provide evidence on the decay mechanisms of glycine and formation pathways of irradiation products such as CH_3NH_2 upon exposure to energetic electrons. Pure glycine-1- ^{12}C ($\text{H}_2\text{NCH}_2\text{COOH}$, Sigma Aldrich, 99+%), glycine-1- ^{13}C ($\text{H}_2\text{NCH}_2^{13}\text{COOH}$, Sigma Aldrich, 99%), glycine- d_5 ($\text{D}_2\text{NCD}_2\text{COOH}$, CDN Isotopes, 98.4%), glycine-N,N,O- d_3 ($\text{D}_2\text{NCH}_2\text{COOD}$, Sigma Aldrich, 98%), glycine-2,2- d_2 ($\text{H}_2\text{NCD}_2\text{COOH}$, CDN Isotopes, 98.6%), and $\text{Mg}(\text{ClO}_4)_2 \cdot 6\text{H}_2\text{O}$ (Sigma Aldrich, 99.0+%) were used to prepare thin films on the silver substrate (Table 1). In their zwitterionic form, glycine- d_5 and glycine-N,N,O- d_3 transfer their deuterium atoms from the carboxylic group to the amino groups ($^+\text{D}_3\text{NCD}_2\text{COO}^-$, $^+\text{D}_3\text{NCH}_2\text{COO}^-$), therefore the latter will be referred as glycine-N,N,N- d_3 throughout the text.

The samples were prepared exploiting the method established by Góbi et al. (2016a). In short, pure glycine or glycine-1- ^{13}C and $\text{Mg}(\text{ClO}_4)_2 \cdot 6\text{H}_2\text{O}$ for the glycine-1- ^{13}C - $\text{Mg}(\text{ClO}_4)_2 \cdot 6\text{H}_2\text{O}$ mixtures were dissolved in a molar ratio of 3:1 or 5:1 in distilled water (H_2O), or in deuterium oxide (D_2O , Cambridge Isotopes, 99.9%) if the sample material was glycine- d_5 or glycine-N,N,N- d_3 . Thereafter, 0.25–0.35 ml of the respective solution was put onto the surface of the silver substrate. The solvent was then allowed to evaporate by heating the substrate to 323–333 K. Care has to be taken in the case of glycine- d_5 and glycine-N,N,N- d_3 because they can easily exchange the deuterium of their amino groups with hydrogen from water vapor; therefore these samples were prepared under a D_2O -rich atmosphere. The average sample thicknesses were estimated by knowing the volume of the solution added on the silver surface and the average densities of the sample and the silver (Table 1). The samples were then placed into the main chamber; after evacuation the chamber was baked then cooled down to 5.5 K. During the “bake-out” the temperature of the sample inside did not exceed 320 K. This temperature is high enough to eliminate all volatile molecules stuck on the surface of the inner wall of our chamber in UHV conditions but low enough to prevent the sublimation of the glycine molecules in the sample. Nevertheless, FTIR spectra were taken of all samples right after their preparation, then before and after “baking,” and no changes could be observed in any cases. The samples were then bombarded with 5 keV electrons isothermally at 5.5 ± 0.1 K for 1 hr at 25.5 ± 1.5 nA (Table 2) over an area of 1.0 ± 0.1 cm^2 at an angle of incidence of 70° relative to the surface normal. This results in a total exposure of the samples of 6×10^{14} electrons cm^{-2} . The emission current was measured prior to and after irradiation utilizing a Faraday cup (Kimball Physics, FC-71) mounted inside the main chamber. The average dose per molecule deposited into the sample was determined via Monte Carlo (CASINO) simulations (Drouin et al. 2007, see also Table 2) to be 9.30 ± 1.10 eV per glycine molecule and 39.39 ± 4.59 eV per $\text{Mg}(\text{ClO}_4)_2 \cdot 6\text{H}_2\text{O}$ molecule. These doses correspond to an exposure time of the soil 5–10 cm below the Martian surface of approximately 240 million years (Pavlov et al. 2012). The

calculated average penetration depth of the energetic electrons (180 nm, Table 2) is less than the thickness of the thinnest sample (450 nm); therefore, the electrons interact only with the deposited sample molecules and not with the silver substrate. Blank experiments (without irradiation) were also carried out in order to monitor potential contaminants.

The irradiation-induced chemical processing of the samples was monitored online and in situ throughout the duration via an FTIR spectrometer (FTIR; Nicolet 6700) from 6000 to 400 cm^{-1} at a resolution of 4 cm^{-1} . Each spectrum was recorded for two minutes, resulting in a set of 30 infrared spectra during the radiation exposure for each system. Although integrated band areas can be altered by optical interference effects, this issue is circumvented by the integration of weak bands, whose absorbance remains linear with respect to the thickness of the sample. After the irradiation, the sample was kept at 5.5 ± 0.1 K for one hour; then temperature-programmed desorption (TPD) studies were conducted by heating the irradiated ices at a rate of 1.0 K min^{-1} to 300 K. This was followed by an isothermal phase at 300 K for additional 3 hr to allow any potential product to diffuse out of the sample into the gas phase. Throughout the thermal sublimation process, the molecules were monitored using a PI-ReTOF-MS instrument (Jordan TOF Products Inc.) (Jones & Kaiser 2013). Products were ionized upon sublimation via single-photon ionization with coherent vacuum ultraviolet (VUV) light. Pulsed VUV light at 118.2 nm (10.49 eV) was generated via nonlinear four-wave mixing ($\omega_{\text{VUV}} = 3\omega_1$) utilizing xenon (Xe) gas as the nonlinear medium (Hilbig & Wallenstein 1981, Maity et al. 2014). Here, ω_1 represents the fundamental frequency from the third-harmonic (354.6 nm) output of a high-power pulsed neodymium-doped yttrium aluminum garnet laser (Nd:YAG, Spectra Physics, PRO-250, 30 mJ per pulse) operated at 30 Hz. A pulsed valve was housed in a doubly differentially pumped chamber evacuated by a 400 L s^{-1} turbomolecular pump held at typically 2×10^{-4} mbar when operated at 30 Hz, -400 V, and 80 μs opening time. The pulsed valve fired 200 μs prior to the Q -switch of the Nd:YAG laser to release the xenon gas at a backing pressure of 1266 Torr (99.999%; Specialty Gases of America) in a T-shaped stainless steel adapter with 1 mm diameter at 25 mm length in line with the propagating laser beam (354.6 nm). The generated VUV light was then separated from the fundamental ω_1 beam by utilizing an off-axis mounted plano-convex lithium fluoride (LiF) lens (ISP Optics, LF-PX-38-150) (VonDrasek et al. 1988, Maity et al. 2014). The ionizing VUV beam passed the ice surface at a distance of 1 mm facing the entrance aperture of the ReTOF. Molecular ions were detected utilizing a multichannel plate with a dual chevron configuration, and the signal was amplified using a fast preamplifier (Ortec 9306) and shaped with a 100 MHz discriminator (Advanced Research Instruments, F-100TD). Once the molecules thermally sublime, they are ionized by VUV light via single-photon ionization and mass-analyzed based on their arrival times. The ReTOF spectra were recorded with a personal-computer-based multichannel scaler (FAST ComTec, P7888-1 E) using a bin width of 4 ns, triggered at 30 Hz (Quantum Composers, 9518) with 3600 sweeps per mass spectrum correlated with a change in temperature of 1 K per minute.

Table 1
Summary of Preparation Details of Glycine-1-¹²C, its Isotopologues, and Glycine-1-¹³C–Mg(ClO₄)₂ · 6H₂O 5:1 and 3:1 Samples

	Glycine-1- ¹² C	Glycine-1- ¹³ C	Glycine-d ₅	Glycine-N,N,N-d ₃	Glycine-2,2-d ₂	Glycine-1- ¹³ C–Mg(ClO ₄) ₂ · 6H ₂ O	
						5:1	3:1
Mass of glycine weighed (g)	0.0107 ± 0.0001	0.0100 ± 0.0001	0.0305 ± 0.0001	0.0286 ± 0.0001	0.0322 ± 0.0001	0.0060 ± 0.0001	0.0060 ± 0.0001
Mass of Mg(ClO ₄) ₂ · 6H ₂ O weighed (g)	0.0000 ± 0.0000	0.0000 ± 0.0000	0.0000 ± 0.0000	0.0000 ± 0.0000	0.0000 ± 0.0000	0.0050 ± 0.0001	0.0086 ± 0.0001
Mass of solvent H ₂ O/D ₂ O (g)	42.20 ± 0.01	42.18 ± 0.01	25.05 ± 0.01 ^a	25.32 ± 0.01 ^a	25.30 ± 0.01	25.12 ± 0.01	25.05 ± 0.01
Mg(ClO ₄) ₂ · 6H ₂ O to glycine molar ratio	0.191 ± 0.005	0.329 ± 0.007
Volume of solution used (mL)	0.35 ± 0.05	0.35 ± 0.05	0.25 ± 0.05	0.25 ± 0.05	0.25 ± 0.05	0.36 ± 0.05	0.35 ± 0.05
Average thickness of sample (nm)	550 ± 80	510 ± 70	2100 ± 50	1950 ± 50	1970 ± 50	900 ± 90	1130 ± 120
Average density of film (g cm ⁻³)	1.61 ± 0.01 ^b	1.61 ± 0.01 ^c	1.61 ± 0.01 ^c	1.61 ± 0.01 ^c	1.61 ± 0.01 ^c	1.76 ± 0.01 ^d	1.81 ± 0.02 ^d
Molar masses of molecules in film (g mol ⁻¹)	75.07	76.07	80.10	78.09	77.08	76.07 ^e	76.07 ^e
						331.30 ^f	331.30 ^f
Number of molecules in sample (×10 ¹⁷)	7.10 ± 1.02	6.64 ± 0.96	25.4 ± 0.7	24.2 ± 0.6	24.8 ± 0.7	6.82 ± 0.70 ^e	6.65 ± 0.69 ^e
						1.30 ± 0.13 ^f	2.19 ± 0.23 ^f

Notes.

^a D₂O was used as solvent.

^b Houck (1930).

^c Due to lack of data the densities of isotopologues were assumed to be equal to those of normal glycine.

^d To calculate the average value the density of Mg(ClO₄)₂ · 6H₂O was assumed to be 1.98 ± 0.03 g cm⁻³ (Lewis 2007).

^e Glycine-1-¹³C.

^f Mg(ClO₄)₂ · 6H₂O.

Table 2
Summary of CASINO Simulations on the Electron Radiolysis Experiments of Glycine-1-¹²C, its Isotopologues, and Glycine-1-¹³C–Mg(ClO₄)₂ · 6H₂O 5:1 and 3:1 Samples

	Glycine-1- ¹² C	Glycine-1- ¹³ C	Glycine-d ₅	Glycine-N,N,N-d ₃	Glycine-2,2-d ₂	Glycine-1- ¹³ C–Mg(ClO ₄) ₂ · 6H ₂ O	
						5:1	3:1
Angle of incidence (deg)	70	70	70	70	70	70	70
Irradiated area (cm ²)	1.0 ± 0.1	1.0 ± 0.1	1.0 ± 0.1	1.0 ± 0.1	1.0 ± 0.1	1.0 ± 0.1	1.0 ± 0.1
Irradiation time (s)	3600 ± 2	3600 ± 2	3600 ± 2	3600 ± 2	3600 ± 2	3600 ± 2	3600 ± 2
Applied electron current (nA)	25.5 ± 0.5	25.0 ± 1.2	24.0 ± 1.0	24.5 ± 1.4	25.0 ± 1.2	26.5 ± 0.8	27.0 ± 3.5
Number of electrons generated (×10 ¹⁴)	5.73 ± 0.11	5.61 ± 0.26	5.39 ± 0.23	5.50 ± 0.31	5.61 ± 0.25	5.95 ± 0.18	6.06 ± 0.79
Initial energy of the electrons (keV)	5.00	5.00	5.00	5.00	5.00	5.00	5.00
Average backscattered energy of the electrons (keV)	3.31 ± 0.08	3.31 ± 0.08	3.31 ± 0.08	3.31 ± 0.08	3.31 ± 0.08	3.37 ± 0.08	3.38 ± 0.07
Average transmitted energy of the electrons (keV)	0.00 ± 0.00	0.00 ± 0.00	0.00 ± 0.00	0.00 ± 0.00	0.00 ± 0.00	0.00 ± 0.00	0.00 ± 0.00
Fraction of backscattered electrons (%)	35.5 ± 2.5	35.5 ± 2.5	35.5 ± 2.5	35.5 ± 2.5	35.5 ± 2.5	36.9 ± 1.0	37.5 ± 1.1
Fraction of transmitted electrons (%)	0.0 ± 0.0	0.0 ± 0.0	0.0 ± 0.0	0.0 ± 0.0	0.0 ± 0.0	0.0 ± 0.0	0.0 ± 0.0
Simulated average penetration depth (nm)	180 ± 7	180 ± 7	180 ± 7	180 ± 7	180 ± 7	177 ± 1	175 ± 3
Number of exposed molecules (×10 ¹⁷)	2.33 ± 0.25	2.30 ± 0.25	2.18 ± 0.24	2.18 ± 0.24	2.27 ± 0.24	1.34 ± 0.14 ^a 0.26 ± 0.03 ^b	1.03 ± 0.11 ^a 0.34 ± 0.04 ^b
Dose per molecule (eV)	9.40 ± 1.05	9.34 ± 1.11	9.44 ± 1.11	9.39 ± 1.17	9.46 ± 1.12	9.06 ± 0.96 ^a 39.47 ± 4.17 ^b	9.02 ± 1.15 ^a 39.30 ± 5.00 ^b

Notes.

^a Glycine-1-¹³C.

^b Mg(ClO₄)₂ · 6H₂O.

3. Results

3.1. Infrared Spectrum of Glycine and Glycine–Mg(ClO₄)₂ · 6H₂O Samples

The FTIR spectra of the samples between 4000 and 500 cm^{−1} before and after the irradiation are shown in Figure 1. The assignment of the most important bands of zwitterionic glycine was discussed in detail in Góbi et al. (2016a) and shows excellent agreement with the FTIR spectrum of the pure glycine sample (Figure 1(a)). Also, the spectra of glycine-1-¹³C–Mg(ClO₄)₂ · 6H₂O 5:1 (Figure 1(c)) and 3:1 (Figure 1(d)) show similarities with the glycine–Mg(ClO₄)₂ · 6H₂O mixture used in our previous experiments (Góbi et al. 2016a). Similarly, some particular characteristic frequencies are shifted toward lower wavenumbers in the deuterated samples (Figures 1(e) and (f)). As a consequence, the positions of these shifted vibrational modes are much closer to each other than in the hydrogen-containing samples.

Upon irradiation with energetic electrons, a ubiquitous decrease and broadening of the IR bands is observed (“before” and “after” spectra in Figure 1). Worth noting is that the blank experiment did not show any changes. There is only one new peak emerging in all samples, at 2345 cm^{−1}, or at 2278 cm^{−1} if the sample contains glycine-1-¹³C, belonging to CO₂. However, in glycine-d₅ and glycine-N,N,N-d₃ they are superimposed by the large absorptions of the Fermi-resonance bands of glycine shifted toward lower wavenumbers. It is also important to point out that in all ¹³C-containing samples (even in the mixtures with Mg(ClO₄)₂ · 6H₂O) *only* the formation of carbon-¹³C dioxide (¹³CO₂) at 2278 cm^{−1} was detected; no evidence for the presence of carbon-¹²C dioxide (¹²CO₂) was found. Contrary to our previous results, the signals of the

stretching vibration of carbon monoxide ($\nu^{12}\text{CO}$, or $\nu^{13}\text{CO}$ in ¹³C-containing samples at 2140 or 2100 cm^{−1}) are very weak and hidden in the isotopologue samples by the glycine bands and thus cannot be observed. All observed IR bands and their assignments can be found in Tables 6–9 in the Appendix.

3.2. TPD Profiles of Glycine and Glycine–Mg(ClO₄)₂ · 6H₂O Samples

3.2.1. Pure Glycine-1-¹²C- and Glycine-1-¹³C

After the irradiation, all samples were heated to 300 K while their TPD profiles were collected at a photoionization energy of 10.49 eV; the data clearly reveal that both non-deuterated pure glycine samples depict a very similar TPD pattern (Figures 2(a) and (b)). A signal at $m/z = 75$ (and 76 for the glycine-1-¹³C, blue lines in Figures 2(a) and (b)) starts at approximately 260 K, whereas the peak with the highest intensity can be found at $m/z = 30$ (red). Additional ion counts are evident at $m/z = 31$ (dark yellow) from 180 to 190 K and at $m/z = 17$ (black) starting at 240–250 K, respectively.

3.2.2. Glycine-d₅, Glycine-N,N,N-d₃, Glycine-2,2-d₂

The deuterated samples have TPD profiles showing similar features to the non-labeled one. The irradiated glycine-d₅, Figure 2(e)) system depicts a signal at $m/z = 80$ (blue); ion counts can also be seen at $m/z = 36$ (dark yellow), at $m/z = 34$ (red), and at $m/z = 20$ (black). The corresponding peaks for the partially deuterated non-zwitterionic glycine-N,N,N-d₃ (Figure 2(f)) are at $m/z = 78$ (blue), and at m/z values of 34 (dark yellow), 33 (orange), 32 (red), 20 (black), and 19 (gray), respectively.

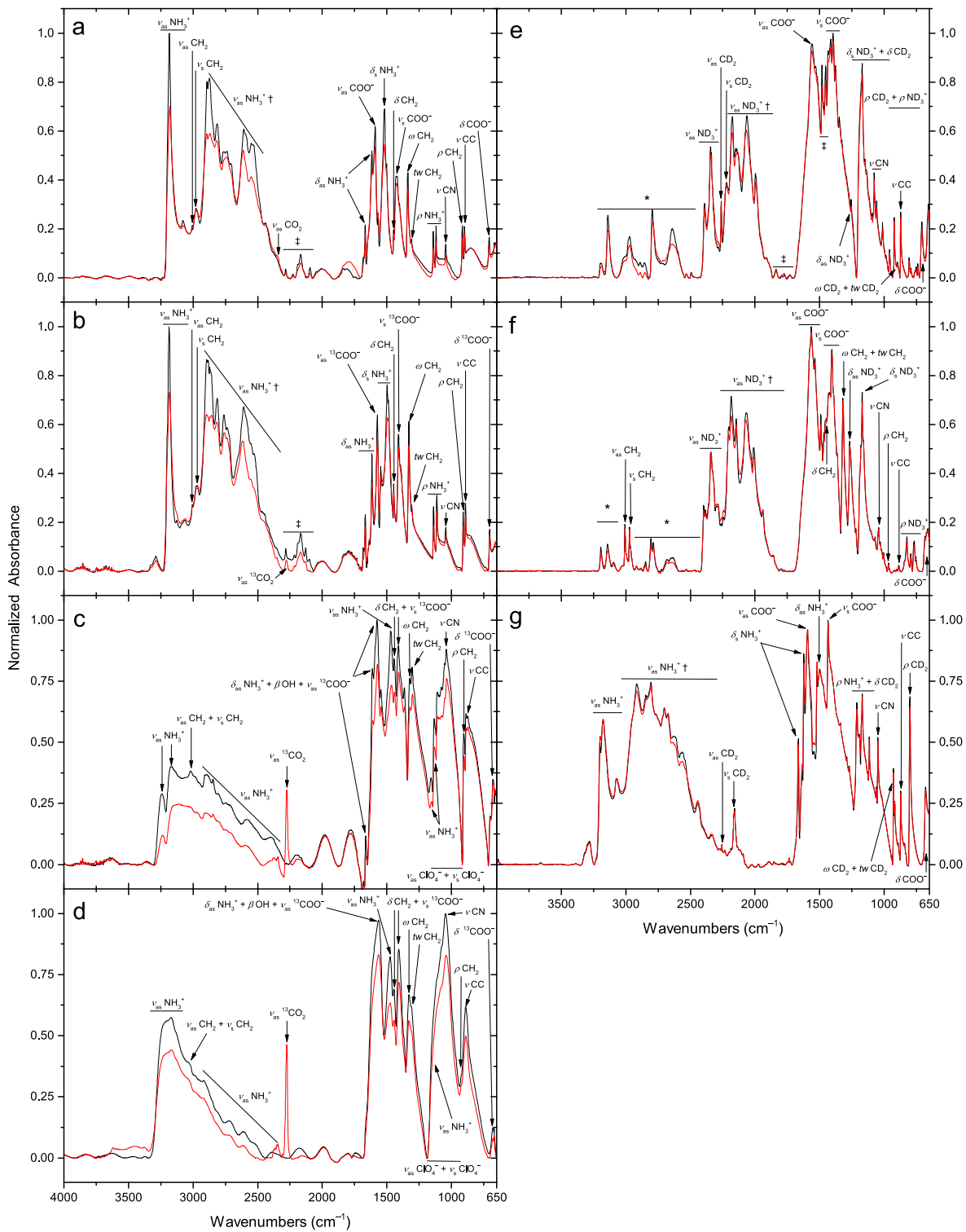


Figure 1. Infrared spectra of (a) glycine-1- ^{12}C , (b) glycine-1- ^{13}C , (c) glycine-1- ^{13}C - $\text{Mg}(\text{ClO}_4)_2 \cdot 6\text{H}_2\text{O}$ 5:1, (d) glycine-1- ^{13}C - $\text{Mg}(\text{ClO}_4)_2 \cdot 6\text{H}_2\text{O}$ 3:1, (e) glycine- d_5 , (f) glycine-N,N,N- d_3 , and (g) glycine-2,2- d_2 before irradiation (black line) and after (red line). The vibrational modes marked on panels (a) to (d) are based on the assignment of Góbi et al. (2016a); for those of the isotopologues (e)–(g) see text and Tables 6–9 in the Appendix. The difference in graphs (e)–(g) between pre-irradiated sample and after irradiation is not that pronounced because of the use of thicker samples. Dagger symbols mean Fermi resonances (†) and combination bands (‡), respectively, while asterisks (*) on (e) and (f) show the signals of H-contaminated glycine isotopologues.

For glycine-2,2- d_2 a signal can be found at $m/z = 77$ in Figure 2(g) (blue), whereas further ion counts can be obtained at $m/z = 33$ (dark yellow), 32 (red), 31 (orange), 18 (gray),

and 17 (black), respectively. It is worth noting that compared to the non-deuterated products, the main peaks are shifted toward m/z values higher by 5, 3, and 2, respectively for glycine- d_5 ,

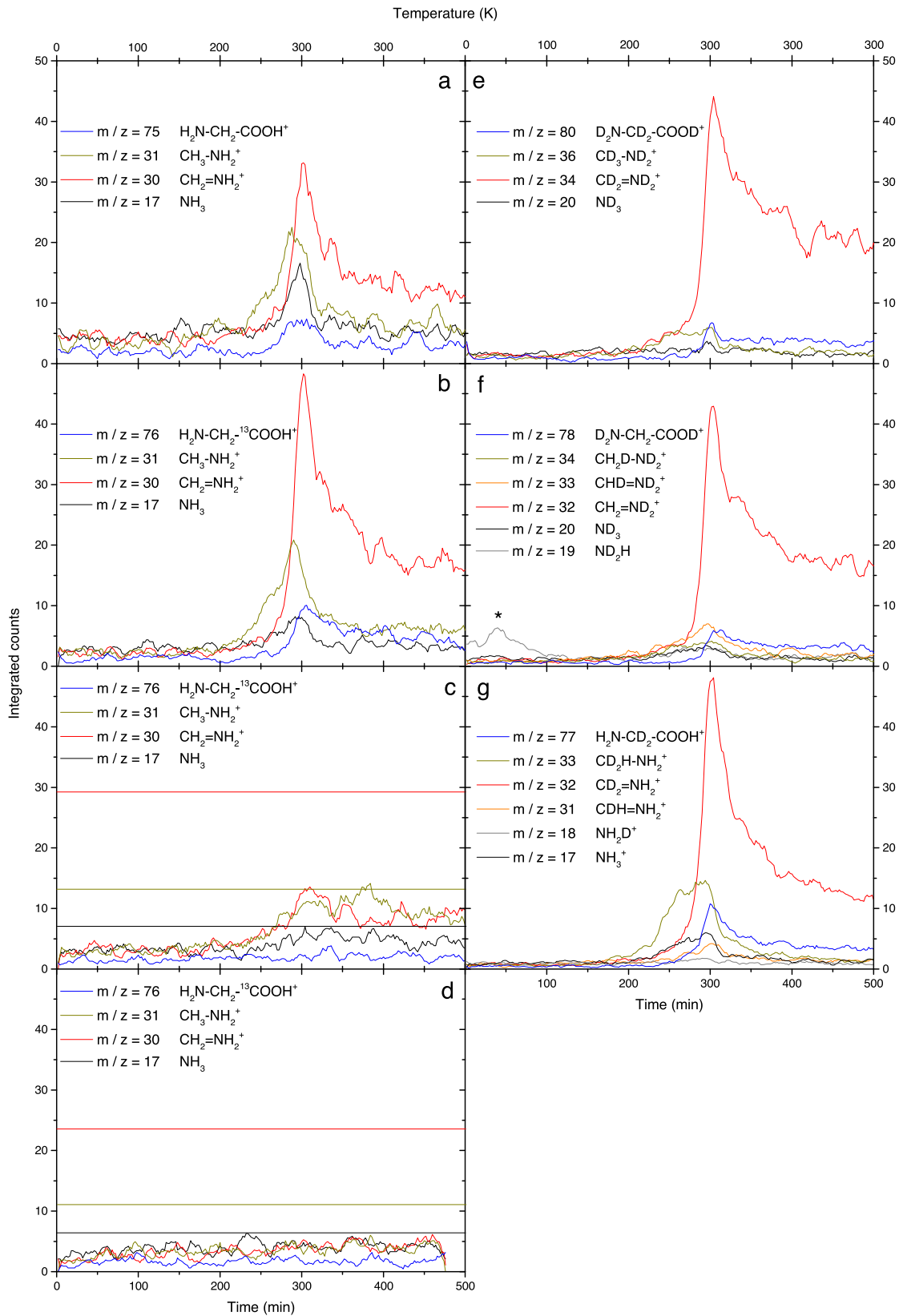


Figure 2. TPD profiles of (a) glycine-1-¹²C, (b) glycine-1-¹³C, (c) glycine-1-¹³C-Mg(ClO₄)₂ · 6H₂O 5:1, (d) glycine-1-¹³C-Mg(ClO₄)₂ · 6H₂O 3:1, (e) glycine-d₅, (f) glycine-N,N,N-d₃, (g) and glycine-2,2-d₂ irradiation products, respectively. See detailed explanation on the product species for different m/z values in the text. The horizontal lines (dark yellow: $m/z = 31$, red line: $m/z = 30$, and black line: $m/z = 17$) for the glycine-1-¹³C-Mg(ClO₄)₂ · 6H₂O mixtures in (c) and (d) show the theoretical signal maxima calculated by multiplying those of the pure glycine samples by the ratio of the glycine mass in that particular mixture of glycine to that of the pure sample. The asterisk on panel (f) marks the contaminant species H_3O^+ ($m/z = 19$).

glycine-N,N,N-d₃, and glycine-2,2-d₂, respectively. This confirms that the molecules formed have five, three, and two hydrogen/deuterium atoms, respectively.

3.2.3. Glycine-1-¹³C-Mg(ClO₄)₂ • 6H₂O

Figures 2(c) and (d) depict the TPD profiles of the products sublimed from the irradiated glycine-1-¹³C-Mg(ClO₄)₂ • 6H₂O 5:1 and 3:1 mixtures. The horizontal lines define the expected signal level based on the pure glycine-1-¹³C experiments adjusted for the depletion fraction in the present experiments. As can be seen, the majority of the radiolysis products detected in pure glycine samples disappeared and/or decreased in intensity; however, no new species could be identified at all.

4. Discussion

4.1. Interpretation of the Infrared Spectra

Assignments of the pure glycine and glycine-Mg(ClO₄)₂ • 6H₂O 1:1 mixture samples are given in Góbi et al. (2016a), whereas those of the isotope-labeled and deuterated glycine samples are summarized in Tables 6–9 in the Appendix. Although the FTIR spectra of glycine-1-¹³C-Mg(ClO₄)₂ • 6H₂O 5:1 (Figure 1(c)) and 3:1 (Figure 1(d)) mixtures agree well with our previous observations on the 1:1 mixture, there are obvious differences. These are the changes in infrared intensity ratios because of the different mixture ratios used during these measurements and the isotopic shifts in vibrational frequencies of glycine caused by the ¹³C atoms of the carboxylic group, respectively. These are also outlined in Figures 1(a) and (b), where differences between the samples containing ¹²C versus ¹³C atoms can be clearly seen.

IR peaks of the deuterated samples (Figures 1(e) and (f)) are also shifted toward shorter wavelengths, indicating the functional groups with the heavier deuterium atoms. However, it is important to note that due to this shift the positions of these vibrational modes are much closer to each other than in the hydrogen-containing samples. Consequently, the assignment of the deuterated samples becomes extremely difficult in the region below 1200 cm⁻¹. This phenomenon was reported earlier, and despite the extensive research on this topic there is still no consent yet on the correct assignments of these modes (Suzuki et al. 1963; Grenie & Garrigou-Lagrange 1972, Herranz & Delgado 1975, Barlow et al. 1998). It is also important to note that since the glycine-d₅ and glycine-N,N,N-d₃ samples are prone to exchange their deuterium atoms on their amino group quickly, partially hydrogenated positions can be seen in the IR spectrum (marked with asterisks in Figures 1(e) and (f)). These might be formed while the sample was being inserted in the main chamber and the system was pumped down; based on the FTIR absorbance, their ratios to the intact sample molecules are roughly 0.2 for glycine-d₅ and 0.1 for glycine-N,N,N-d₃, respectively.

Upon irradiation, the general decrease and broadening of the glycine IR bands is caused by the simultaneous decomposition, amorphization, and polymerization of the samples (Góbi et al. 2016a). As has already been pointed out in our earlier work, the ubiquitous broadening can also be caused by the formation of various irradiation products such as CH₃NH₂ (reaction R1), CH₄ (reaction R3), and NH₃ (reaction R4). However, their FTIR signals can only be assigned tentatively, and the use of more sensitive analytical methods (PI-ReTOF-MS) is necessary to detect at least some of these products without any doubt. The only emerging peak at 2345 cm⁻¹ is that of the antisymmetric

stretching vibration of carbon dioxide ($\nu_{\text{as}} \text{CO}_2$); the same peak in ¹³C-labeled samples can be found at 2278 cm⁻¹ ($\nu_{\text{as}} \text{ } ^{13}\text{CO}_2$). Furthermore, the fact that in the samples containing ¹³C atoms only the formation of ¹³CO₂ can be observed implies a specific decomposition mechanism as discussed in detail in Section 4.3.3.

4.2. Interpretation of the TPD Profiles

4.2.1. Pure Glycine-1-¹²C and Glycine-1-¹³C

The peaks at $m/z = 75$ (Figure 2(a), blue) and 76 (Figure 2(b), blue) belong to the parent molecular ions of glycine-1-¹²C (H₂NCH₂¹²COOH⁺) and glycine-1-¹³C (H₂NCH₂¹³COOH⁺), respectively. Their adiabatic ionization energies (IEs) are 9.21 ± 0.05 eV (Zaretskii et al. 1971) or 8.9 eV (Cannington & Ham 1983). It is important to note that the glycine molecule in the gas phase has a non-zwitterionic structure (H₂NCH₂COOH), whereas glycine in the crystal is zwitterionic (⁺H₃NCH₂COO⁻). The signals at $m/z = 31$ (Figures 2(a) and (b), dark yellow) and 17 (Figures 2(a) and (b), black) can easily be associated with CH₃NH₂⁺ (IE = 8.9 ± 0.1 eV, Aue et al. 1976) and with NH₃⁺ (IE = 10.069 ± 0.002 eV, Loch et al. 1992), respectively. From these the latter may originate either from the electron irradiation of zwitterionic glycine (the so-called deamination process) or from the radiolysis of CH₃NH₂ (reaction R4). It is important to stress that neither the photofragmentation of non-zwitterionic glycine (Jochims et al. 2004) nor that of CH₃NH₂ (Yang et al. 2012) can produce NH₃. The CH₃NH₂ forms via decarboxylation (^{12/13}CO₂ loss) of the parent glycine molecule upon electron irradiation (reaction R1).

The origin of the peak with the highest intensity ($m/z = 30$, red lines on Figures 2(a) and (b)) is even more intriguing and belongs to methyleneimmonium ions (CH₂=NH₂⁺). If considering the TPD profiles, it can be seen that this signal may originate from photofragmentation of non-zwitterionic glycine and/or from CH₃NH₂. Both pathways are feasible because the appearance energy during VUV fragmentation of the former molecule is 10.27 ± 0.05 eV (Zaretskii et al. 1971); for the latter, the appearance energy is more uncertain and varies between 10.18 eV (Lossing et al. 1981) and 10.82 ± 0.15 eV (Collin & Franskin 1966). However, these appearance energies and the fact that the signal shape is similar to that of the glycine suggest its origin. Therefore we propose that this signal can be connected to the CH₂=NH₂⁺ ions formed via photofragmentation of the non-zwitterionic glycine molecule (via ^{12/13}COOH loss) itself with a smaller contribution from the CH₃NH₂ by hydrogen atom loss. This can also explain the relatively low intensity of the parent molecule's signal at $m/z = 75$ (or 76 for the carbon-¹³C sample, blue in Figures 2(a) and (b)). It is also important to note that no other photofragments of glycine are expected because their appearance energies are higher than the photoionization energy used (10.49 eV). Also, there is an alternative structure besides the CH₂=NH₂⁺ ion at $m/z = 30$. This may be formed by losing a hydrogen atom from the amino group (methylnitrenium ion, CH₃NH⁺); however, this ion is not expected to be stable (Jochims et al. 2004). Worth noting is that the IEs of the alternative (expected) irradiation products such as CO₂ ($m/z = 44$, 13.776 ± 0.008 eV, Parr & Taylor 1974), CH₄ ($m/z = 16$, 12.61 ± 0.01 eV, Berkowitz et al. 1987), and possibly imidogen (NH, $m/z = 15$, 12.8, or 13.480 ± 0.002 eV, depending on the data source, Melton 1966; Garcia et al. 2015) are higher than the photoionization energy used (10.49 eV). As a consequence their signal cannot be obtained. The other product of reaction R4

besides NH_3 is methylene (CH_2 , $m/z = 14$, 10.393 ± 0.011 eV, Litorja & Ruscic 1998). Although it has an IE low enough, which would allow its detection, we cannot observe it. The reason is that it reacts further even before the collection of the TPD profile owing to its high reactivity (Tsegaw et al. 2016). A summary of the detected species and their possible origins for all pure glycine samples is given in Table 3.

4.2.2. Glycine- d_5 , Glycine- $N,N,N-d_3$, Glycine-2,2- d_2

Similar conclusions can be drawn for the deuterated glycine isotopologues to those for their non-deuterated derivative. For glycine- d_5 (Figure 2(e)) there is a signal at $m/z = 80$ (blue), which corresponds to the non-zwitterionic molecular ion ($\text{D}_2\text{NCD}_2\text{COOD}^+$). Deuterated methylamine- d_5 molecular ion (CD_3ND_2^+) can be traced at $m/z = 36$ (dark yellow), whereas the peak of the photofragmentation product, i.e., the methyleneimmonium- d_4 ion ($\text{CD}_2=\text{ND}_2^+$) can be found at $m/z = 34$ (red). Ion counts of ammonia- d_3 cations (ND_3^+) can also be detected at $m/z = 20$ (black).

Glycine- $N,N,N-d_3$ (Figure 2(f)) has peaks at m/z values of 78 (blue) and 34 (dark yellow) that belong to the parent molecular ion ($\text{D}_2\text{NCH}_2\text{COOD}^+$) and methyl- d_1 -amine- $N,N-d_2$ ($\text{CH}_2\text{DND}_2^+$). Ion counts at $m/z = 33$ (orange) and 32 (red) can also be traced, with the former one as the photofragmentation product of the methylamine isotopologue ($\text{CH}_2\text{DND}_2^+$) by hydrogen atom loss. Accordingly, the latter one is either the photofragmentation product of the $\text{CH}_2\text{DND}_2^+$ via deuterium atom loss or alternatively that of the parent molecule after COOD loss. By comparing the signal strengths of $m/z = 33$ and 32 one can see that the latter one is more intense, indicating that photofragmentation of glycine is preferred over that of the $\text{CH}_2\text{DND}_2^+$. Furthermore, fully and partially deuterated ammonia molecules could be observed as well (ND_3^+ and ND_2H^+ , $m/z = 20$ and 19, black and gray).

The TPD profile glycine-2,2- d_2 (Figure 2(g)) sample shows the peak of the parent molecular ion at $m/z = 77$ ($\text{H}_2\text{NCD}_2\text{COOH}^+$, blue), whereas that of the methyl- d_2 -amine cation $\text{CD}_2\text{HNNH}_2^+$ can be detected at $m/z = 33$ (dark yellow). The ion counts at m/z values 32 (red) and 31 (orange) are those of the partially deuterated methyleneimmonium ions ($\text{CD}_2=\text{NH}_2^+$ and $\text{CDH}=\text{NH}_2^+$, red and orange, respectively). The former one is the fragmentation product of the parent molecular ion (by COOH loss) or formed by hydrogen atom loss of $\text{CD}_2\text{HNNH}_2^+$ cation. The latter originates from the same methylamine isotopologue ($\text{CD}_2\text{HNNH}_2^+$) by deuterium atom loss, resulting in $\text{CDH}=\text{NH}_2^+$. When comparing the signal strengths of $m/z = 32$ and 31 similar conclusions can be drawn as for glycine- $N,N,N-d_3$: photofragmentation of glycine is preferred over that of the $\text{CD}_2\text{HNNH}_2^+$. Ammonia and its deuterated isotopologue (NH_3^+ and NH_2D^+) at $m/z = 17$ and 18 (black and gray) can also be detected as irradiation products.

It is also worth noting that the partially hydrogenated contaminations mentioned in the FTIR results (Section 4.1) can also be detected in the TPD profile of glycine- d_5 (Figure 2(e)). This especially applies to the one that exchanged one deuterium for hydrogen ($^+\text{D}_2\text{HNCND}_2\text{COO}^-$), but its signal can be distinguished easily from those of the unmodified samples since their m/z values are uneven (i.e., at 79, 35, 33, and 19, respectively). For the glycine- $N,N,N-d_3$ samples the concentration of partially hydrogenated compounds was much lower, and glycine-2,2- d_2 does not exchange its deuterium atoms. Thus the signals of contaminants in the TPD profiles were much lower in the case of glycine- $N,N,N-d_3$ than those of the intact molecules or, for glycine-2,2- d_2 , do not pose a

problem at all. Nevertheless, some of the signal at $m/z = 33$ for the former sample may have a contribution from $\text{CH}_2\text{DND}_2^+$ ions after deuterium-hydrogen exchange (i.e., CH_2DNDH^+).

4.2.3. Glycine-1- ^{13}C - $\text{Mg}(\text{ClO}_4)_2 \cdot 6\text{H}_2\text{O}$

The 5:1 mixture (Figure 2(c)) depicts products with lower than expected concentrations based on the measurements on pure samples. It shows that 86% (CH_3NH_2 , $m/z = 31$, dark yellow) and 69% (NH_3 , $m/z = 31$, black) of the molecules were being oxidized most likely by the oxygen atoms originating from the perchlorate units. Our recent PI-ReTOF-MS study of perchlorate mixtures (Góbi et al. 2016b) showed that other oxidants besides oxygen are present in the sample, such as ClO_2 , which is potentially an even more powerful oxidizer than oxygen. However, its signals at m/z values of 67 ($^{35}\text{ClO}_2$) and 69 ($^{37}\text{ClO}_2$) cannot be detected in our irradiated glycine-1- ^{13}C - $\text{Mg}(\text{ClO}_4)_2 \cdot 6\text{H}_2\text{O}$ mixtures, proving that it reacts with the organic molecule and oxidizes it. The lack of glycine decomposition products might be explained by the presence of oxidation products having higher IE than the energy of VUV photons used for photoionization (10.49 eV, see also Section 4.3.3). Moreover, these peaks are completely missing from the 3:1 mixture (Figure 2(d)) owing to the even higher relative concentration of oxidants compared to glycine-1- ^{13}C .

4.3. Decay Mechanisms of Glycine

4.3.1. Pure Glycine-1- ^{12}C and Glycine-1- ^{13}C

The degradation mechanism of pure glycine samples can be seen in Figures 3(a)–(e). Basically, two main decomposition pathways may exist: the first step is deamination, i.e., the loss of NH_3 and decarboxylation (reaction R1) that results in the formation of carbon dioxide ($^{12}\text{CO}_2$, or $^{13}\text{CO}_2$ if the sample is labeled with carbon- ^{13}C atoms). The other deamination product is the unstable acetate zwitterion ($^+\text{CH}_2\text{COO}^-$), whereas decarboxylation yields CH_3NH_2 besides CO_2 after a shift of a proton (Figure 3). The $^+\text{CH}_2\text{COO}^-$ can lose carbon dioxide ($^{12}\text{CO}_2$ or $^{13}\text{CO}_2$) with the formation of the end-product CH_2 radical, while CH_3NH_2 can be radiolyzed eventually to NH_3 and CH_2 radical (according to reaction R4) or to CH_4 and NH (reaction R3). As it was already pointed out in Section 3.2, from these four possible end-products (CH_2 radical, NH_3 , CH_4 , and NH) only NH_3 was detected without any doubt. On one hand, NH and CH_4 have IEs too high to be detectable via PI-ReTOF-MS; on the other hand, two of them (CH_2 and NH) are highly reactive and therefore they presumably quickly react further after their formation. Besides, all IR bands of the radiolysis products mainly overlap with those of the parent molecule as well. It is also interesting to note that H_2O loss from matrix-isolated glycine upon UV irradiation along with the formation of aminoketenes ($^+\text{H}_3\text{NCH}=\text{C}=\text{O}$) was also reported previously (Bazsó et al. 2012). However, no evidence could be found for the presence of aminoketenes or their possible degradation product ketene ($\text{H}_2\text{C}=\text{C}=\text{O}$) by IR spectroscopy or PI-ReTOF-MS. A likely explanation for this phenomenon is that glycine molecules were in zwitterionic form ($^+\text{H}_3\text{NCH}_2\text{COO}^-$) in our sample. However, the presence of the protonated carboxylic group is preferred for the water loss, i.e., the non-zwitterionic glycine ($\text{H}_2\text{NCH}_2\text{COOH}$)—as was the case during the matrix-isolation experiments of Bazsó et al. (2012).

Of the two feasible reaction pathways (i.e., deamination and decarboxylation) the second one is more likely to be the main channel. Accordingly, based on our experimental findings,

Table 3
Summary of Species Detected by the PI-ReTOF Mass Spectrometry for the Different Pure Glycine Samples and their Possible Origin

Sample	Species Detected			
	Name	Molecular Formula	m/z	Source
Glycine-1- ¹² C (⁺ H ₃ NCH ₂ COO ⁻)	Glycine-1- ¹² C molecular ion	H ₂ NCH ₂ COOH ⁺	75	Photoionization of non-zwitterionic glycine-1- ¹² C parent molecule
	Methylamine molecular ion	CH ₃ NH ₂ ⁺	31	Photoionization of methylamine originating from the electron radiolysis of parent molecule
	Methyleneimmonium cation	CH ₂ =NH ₂ ⁺	30	Photofragmentation of parent molecule (COOH loss)
	Ammonia molecular ion	NH ₃ ⁺	17	Photoionization of ammonia originating from the electron radiolysis of methylamine
Glycine-1- ¹³ C (⁺ H ₃ NCH ₂ ¹³ COO ⁻)	Glycine-1- ¹³ C molecular ion	H ₂ NCH ₂ ¹³ COOH ⁺	76	Photoionization of non-zwitterionic glycine-1- ¹³ C parent molecule
	Methylamine molecular ion	CH ₃ NH ₂ ⁺	31	Photoionization of methylamine originating from the electron radiolysis of parent molecule
	Methyleneimmonium cation	CH ₂ =NH ₂ ⁺	30	Photofragmentation of parent molecule (¹³ COOH loss)
	Ammonia molecular ion	NH ₃ ⁺	17	Photoionization of ammonia originating from the electron radiolysis of methylamine,
Glycine-d ₅ (⁺ D ₃ NCD ₂ COO ⁻)	Glycine-d ₅ molecular ion	D ₂ NCD ₂ COOD ⁺	80	Photoionization of non-zwitterionic glycine-d ₅ parent molecule
	Methylamine-d ₅ molecular ion	CD ₃ ND ₂ ⁺	36	Photoionization of methylamine-d ₅ originating from the electron radiolysis of parent molecule
	Methyleneimmonium-d ₄ cation	CD ₂ =ND ₂ ⁺	34	Photofragmentation of parent molecule (COOD loss)
	Ammonia-d ₃ molecular ion	ND ₃ ⁺	20	Photoionization of ammonia originating from the electron radiolysis of methylamine-d ₅
Glycine-N,N,N-d ₃ (⁺ D ₃ NCH ₂ COO ⁻)	Glycine-N,N,O-d ₃ molecular ion	D ₂ NCH ₂ COOD ⁺	78	Photoionization of non-zwitterionic glycine-N,N,N-d ₃ parent molecule
	Methyl-d ₁ -amine-N,N-d ₂ molecular ion	CH ₂ DND ₂ ⁺	34	Photoionization of methyl-d ₁ -amine-N,N-d ₂ originating from the electron radiolysis of parent molecule
	Methylene-d ₁ -immonium-N,N-d ₂ cation	CHD=ND ₂ ⁺	33	Photofragmentation of methyl-d ₁ -amine-N,N-d ₂ (H loss)
	Methyleneimmonium-N,N-d ₂ cation	CH ₂ =ND ₂ ⁺	32	Photofragmentation of parent molecule (COOD loss)
	Ammonia-d ₃ molecular ion	ND ₃ ⁺	20	Photoionization of ammonia-d ₃ originating from the electron radiolysis of methyl-d ₁ -amine-N,N-d ₂
	Ammonia-d ₂ molecular ion	ND ₂ H ⁺	19	Photoionization of ammonia-d ₂ originating from the electron radiolysis of methyl-d ₁ -amine-N,N-d ₂
Glycine-2,2-d ₂ (⁺ H ₃ NCD ₂ COO ⁻)	Glycine-2,2-d ₂ molecular ion	H ₂ NCD ₂ COOD ⁺	77	Photoionization of non-zwitterionic glycine-2,2-d ₂ parent molecule
	Methyl-d ₂ -amine molecular ion	CD ₂ HNH ₂ ⁺	33	Photoionization of methyl-d ₂ -amine originating from the electron radiolysis of parent molecule
	Methylene-d ₂ -immonium cation	CD ₂ =NH ₂ ⁺	32	Photofragmentation of methyl-d ₂ -amine (H loss)
	Methylene-d ₁ -immonium cation	CDH=NH ₂ ⁺	31	Photofragmentation of parent molecule (COOD loss)
	Ammonia-d ₁ molecular ion	NH ₂ D ⁺	18	Photoionization of ammonia-d ₁ originating from the electron radiolysis of methyl-d ₂ -amine
	Ammonia molecular ion	NH ₃ ⁺	17	Photoionization of ammonia originating from the electron radiolysis of methyl-d ₂ -amine

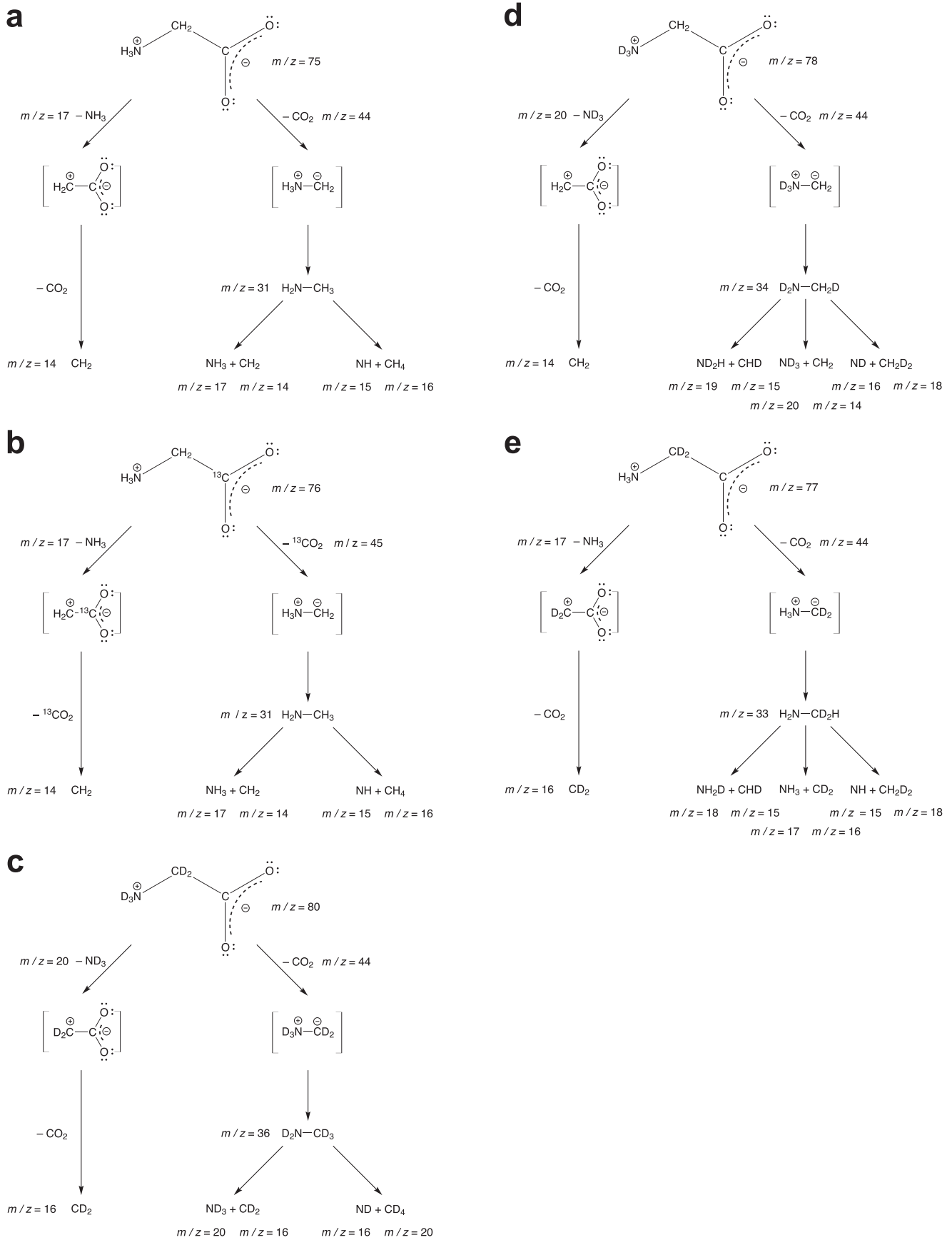


Figure 3. Proposed decomposition pathways of (a) glycine-1-¹²C, (b) glycine-1-¹³C, (c) glycine-d₅, (d) glycine-N,N,N-d₃, and (e) glycine-2,2-d₂ zwitterions.

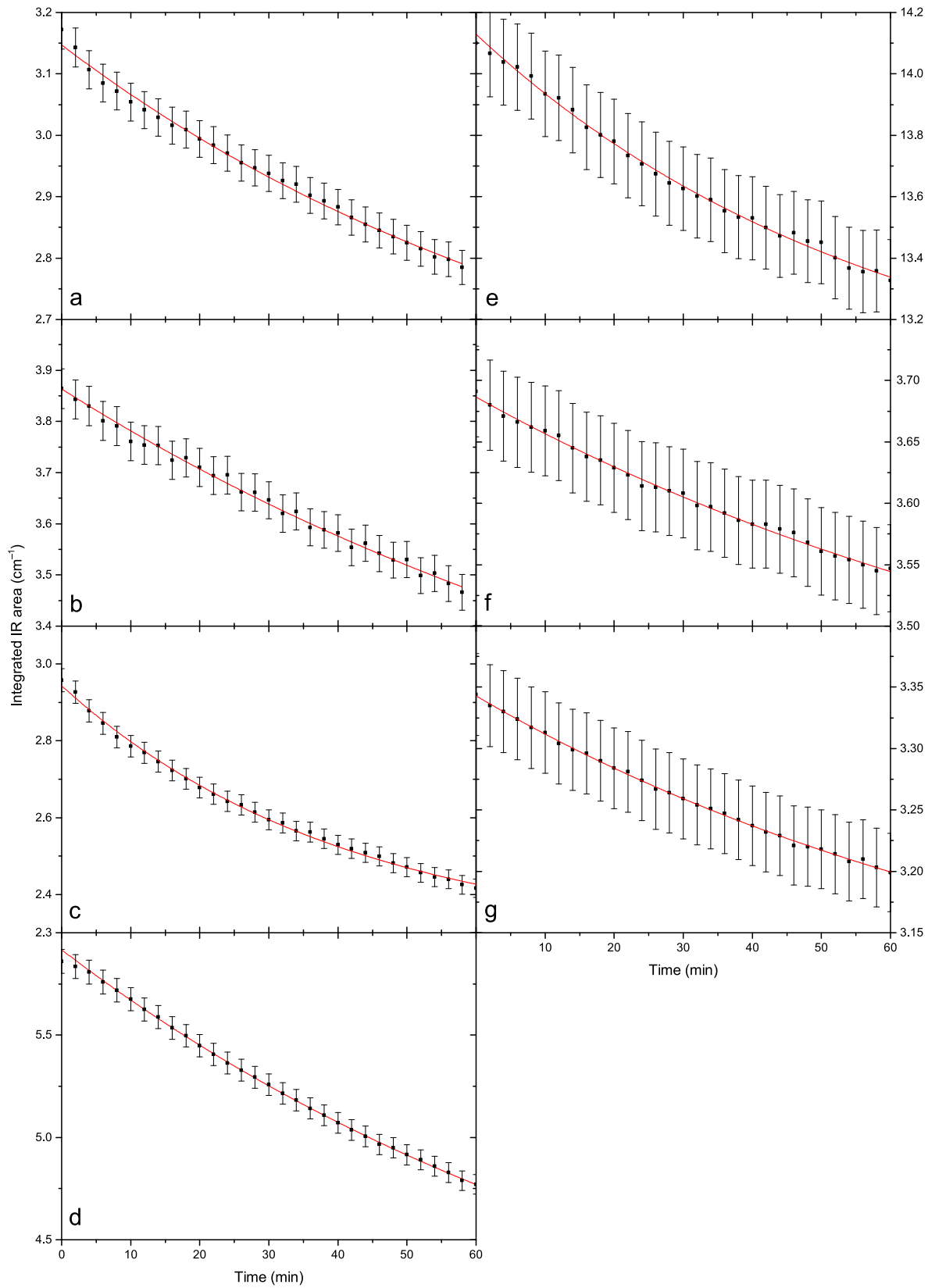


Figure 4. Decay curves of selected IR bands of (a) glycine- $1\text{-}^{12}\text{C}$ ($\delta_s \text{NH}_3$), (b) glycine- $1\text{-}^{13}\text{C}$ ($\delta_s \text{NH}_3$), (c) glycine- $1\text{-}^{13}\text{C}\text{-Mg}(\text{ClO}_4)_2 \cdot 6\text{H}_2\text{O}$ 5:1 ($\delta_s \text{NH}_3$), (d) glycine- $1\text{-}^{13}\text{C}\text{-Mg}(\text{ClO}_4)_2 \cdot 6\text{H}_2\text{O}$ 3:1 ($\delta_s \text{NH}_3$), (e) glycine- d_5 ($\delta_s \text{ND}_3$), (f) glycine- N,N,N-d_3 ($\delta_s \text{ND}_3$), and (g) glycine- $2,2\text{-d}_2$ ($\delta_{\text{as}} \text{NH}_3$) films upon irradiation. For notations of non-deuterated glycine and glycine- $\text{Mg}(\text{ClO}_4)_2 \cdot 6\text{H}_2\text{O}$ vibrational modes see Góbi et al. (2016a); for those of the deuterated glycine species see Tables 6–9 in the Appendix.

Table 4
Decay Rate Constants (in 10^{-4} s^{-1}) of Glycine-1- ^{12}C , its Isotopologues, and Glycine-1- ^{13}C - $\text{Mg}(\text{ClO}_4)_2 \cdot 6\text{H}_2\text{O}$ 5:1 and 3:1 Samples

Sample	Glycine Decay Rate	Ratio of k_{gly} (Mixture) and k_{gly} (Glycine-1- ^{13}C)	CO_2 Formation Rate	Ratio of k_{CO_2} (Mixture) and k_{CO_2} (Glycine-1- ^{13}C)
Glycine-1- ^{12}C	2.10 ± 0.56	...	0.25 ± 0.02	...
Glycine-1- ^{13}C	1.88 ± 0.61	...	0.29 ± 0.03	...
Glycine- d_5	2.22 ± 0.77 ^a	...
Glycine-N,N,N- d_3	1.93 ± 0.54 ^a	...
Glycine-2,2- d_2	2.16 ± 0.76	...	0.22 ± 0.01	...
Glycine-1- ^{13}C - $\text{Mg}(\text{ClO}_4)_2 \cdot 6\text{H}_2\text{O}$ 5:1	2.67 ± 0.31	1.42 ± 0.49	2.55 ± 0.17	8.79 ± 1.08
Glycine-1- ^{13}C - $\text{Mg}(\text{ClO}_4)_2 \cdot 6\text{H}_2\text{O}$ 3:1	3.13 ± 0.46	1.66 ± 0.64	3.06 ± 0.20	10.6 ± 1.3

Note. Decay rate constants are based on experimental IR decay curves. Production rates of CO_2 are given as well.

^a Could not be obtained because of overlap with the high-intensity peak of the ν_{as} ND_3 vibrational mode.

deamination is a less likely reaction pathway. Several observations can substantiate this claim. Most importantly, the concentration of CO_2 molecules in the sample after irradiation is the highest among the product molecules, which may be a sign that it is the very first decay product rather than being a near end-member of a sequential decomposition pathway, as is the case for the deamination reaction. Accordingly, if the loss of NH_3 were the first step it should be the main irradiation product (i.e., it could be detected via IR spectroscopy without any doubt), but its concentration is much lower than that of CO_2 in the sample after the irradiation. Even if it is assumed that the majority of the formed NH_3 reacts further, the higher TPD signal intensity of the other decarboxylation product CH_3NH_2 clearly shows which is the preferred decomposition channel.

CH_3NH_2 can decompose further into various species according to reactions R3 and R4. Of these, the other product besides NH_3 in reaction R4, i.e., the CH_2 radical, quickly reacts with the surrounding molecules. As for the other reaction channel R3, CH_4 can be tentatively identified based on its IR signals, but its IE is too high (Section 4.2.1) for it to be detected by PI-ReTOF-MS. The fate of NH may be similar to that of the CH_2 radical.

4.3.2. Glycine- d_5 , Glycine-N,N,N- d_3 , Glycine-2,2- d_2

The decomposition scheme described in Section 4.3.1 is principally the same for deuterated samples with the corresponding partially or fully deuterated isotopologues. This can be seen in Figures 3(c)–(e). However, it is important to point out further evidence for decarboxylation being the main reaction channel. After amorphization and polymerization, with deamination less likely to occur, partially deuterated ammonia (NH_2D) molecules are present in the glycine-2,2- d_2 sample. If deamination took place first, the exclusive presence of fully hydrogenated NH_3 should be observed. Although similar conclusions could be drawn for the other two deuterated samples in theory, contaminants produced after deuterium–hydrogen exchange on the amino group make an uncertain contribution to the signal of partially deuterated ammonia (e.g., ND_2H).

4.3.3. Glycine-1- ^{13}C - $\text{Mg}(\text{ClO}_4)_2 \cdot 6\text{H}_2\text{O}$

For the samples containing $\text{Mg}(\text{ClO}_4)_2 \cdot 6\text{H}_2\text{O}$ it can be clearly seen from the TPD profiles (Figures 2(c) and (d)) that there must be other reaction channels after (or in parallel to) decarboxylation, which cause the partial or complete lack of the radiolysis products CH_3NH_2 and NH_3 . An obvious possibility is the complete or

partial oxidation of glycine and/or the irradiation products, resulting in an almost 10-fold increase in the decarboxylation rate of glycine-1- ^{13}C as well. In the case of complete oxidation, products such as $^{12}\text{CO}_2$ and nitrogen oxides (N_xO_y) are expected as well. The former product forms when the glycine-1- ^{13}C CH_2 group, CH_3NH_2 methyl group, or CH_2 radicals (reaction R4) are being oxidized. The latter can originate from oxidation of the zwitterionic glycine ammonium group, from the amine group of CH_3NH_2 , from NH_3 or from NH (see also reaction R3). However, neither $^{12}\text{CO}_2$ nor N_xO_y can be detected by FTIR spectroscopy or identified based on the TPD profiles, although CO_2 and nitrous oxide (N_2O , IE = 12.88 ± 0.005 eV, Coppens et al. 1974) have IEs that are too high. However, both nitrogen monoxide (NO , IE = 9.2643 ± 0.0002 eV, Ebata et al. 1983) and nitrogen dioxide (NO_2 , IE = 9.75 ± 0.01 eV, Dibeler et al. 1967) should be detectable with our experimental setup, or else their signals are below the detection limit of the instrument. The reactive radicals formed after oxidation of glycine or its irradiation products can also react with each other yielding, organics similar to polycyclic aromatic hydrocarbons (resulting in the broadening of the IR spectral bands), which may at least partly explain their lack of detection.

Another possible explanation for the results is if partial oxidation of the molecules is assumed: CH_3NH_2 can be transformed into formamide ($\text{H}_2\text{NHC}=\text{O}$) (Fethi et al. 2008) and principally into nitromethane (CH_3NO_2) (Fethi et al. 2008; McCurry et al. 2016). Nevertheless, formation of the latter from CH_3NH_2 in the irradiated sample containing perchlorate anions is most likely to occur because the usually very strong carbonyl vibration signal of the $\text{H}_2\text{NHC}=\text{O}$ cannot be seen in the irradiated IR spectra. Convincing evidence for the decarboxylation being the first step followed by partial oxidation of CH_3NH_2 is the exclusive presence of $^{13}\text{CO}_2$ in these mixture samples. If another reaction occurred first—for instance partial oxidation of the parent molecule glycine-1- ^{13}C or of the deamination products—then the presence of $^{12}\text{CO}_2$ should also be observed as a consequence of the reaction of the other, non-labeled carbon atom on the CH_2 group. However, the IE of CH_3NO_2 (IE = 11.08 ± 0.08 eV, Watanabe et al. 1962) is higher than the photoionization energy used. Therefore, in order to study the behavior of CH_3NH_2 in an oxygen-rich environment and to confirm their radiolysis products, further irradiation experiments have to be done with $\text{CH}_3\text{NH}_2\text{-O}_2$ ice mixtures in the near future.

The idea of (partial) oxidation of the species in the sample containing perchlorate anions cannot solely explain what causes

Table 5
Mass Balance of glycine-1-¹²C, its isotopologues, and Glycine-1-¹³C–Mg(ClO₄)₂ · 6H₂O 5:1 and 3:1 Samples Determined from Experimental IR Decay Curves

Process	Decay Product	Number of Molecules Produced/Decomposed During Irradiation (in 10 ¹⁶ Molecules)						
		Glycine-1- ¹² C	Glycine-1- ¹³ C	Glycine-d ₅	Glycine-N,N,N-d ₃	Glycine-2,2-d ₂	Glycine-1- ¹³ C– Mg(ClO ₄) ₂ · 6H ₂ O 5:1	Glycine-1- ¹³ C– Mg(ClO ₄) ₂ · 6H ₂ O 3:1
⁺ H ₃ NCH ₂ COO [−] → X		12.4 ± 0.4	11.2 ± 0.4	12.2 ± 0.3	11.2 ± 0.3	12.4 ± 0.4	8.19 ± 1.32	6.97 ± 1.32
Fraction of glycine degraded		(53 ± 14)%	(49 ± 16)%	(55 ± 19)%	(50 ± 14)%	(55 ± 19)%	(61 ± 10)%	(68 ± 9)%
ClO ₄ [−] → ClO ₃ [−] + O	O	0.52 ± 0.19 ^c	0.73 ± 0.28 ^c
Number of molecules in sample after irradiation	CO ₂	0.08 ± 0.01	0.11 ± 0.01	0.12 ± 0.04 ^b	0.11 ± 0.04 ^b	0.11 ± 0.01	0.43 ± 0.03	0.86 ± 0.06
	Fraction ^a	(0.65 ± 0.08)%	(0.98 ± 0.10)%	(0.98 ± 0.33)% ^b	(0.98 ± 0.36)% ^b	(0.89 ± 0.09)%	(5.3 ± 0.9)%	(12 ± 2)%
	CH ₃ NH ₂	0.02 ± 0.01	0.02 ± 0.01	0.03 ± 0.01	0.03 ± 0.01	0.02 ± 0.01	0.03 ± 0.01	0.02 ± 0.00
	NH ₃	0.01 ± 0.00	0.02 ± 0.01	0.02 ± 0.01	0.02 ± 0.01	0.02 ± 0.01	<0.01 ± 0.00	<0.01 ± 0.00
	CH ₄	<0.02 ± 0.01	<0.02 ± 0.01	<0.02 ± 0.01	<0.02 ± 0.01	<0.02 ± 0.01	<0.02 ± 0.01	<0.02 ± 0.01
	Fraction ^d	(63 ± 26)%	(55 ± 28)%	(59 ± 32)%	(64 ± 36)%	(55 ± 28)%	(14 ± 5)%	(6 ± 2)%

Notes.

^a Fraction of CO₂ accounting for decomposition of glycine via reaction R1.

^b Bigger uncertainty is due to overlap with the high-intensity peak of the ν_{as} ND₃ vibrational mode.

^c Based on the results of Turner et al. (2016).

^d Fraction of reaction products of reactions R1, R3, and R4 accounting for the CO₂.

the increase in the rate of the initial decarboxylation step. A closer look at reaction R1, however, can answer this question: normally, decomposition of zwitterionic glycine into CH_3NH_2 and CO_2 is an equilibrium process. Therefore, decay products can also transform back into the parent molecule upon electron irradiation (Holtom et al. 2005); it is worth noting that this is possible only because the CO_2 molecules are trapped within the sample due the low temperature used during the experiments. However, if one or both of the radiolysis products is continuously removed from the system (for instance it reacts with the oxygen originating from perchlorate unit), then its back reaction is inhibited. Furthermore an increase in the concentration of the inert product $^{13}\text{CO}_2$ can be observed after the irradiation according to the Le Châtelier–Braun principle. In summary, if glycine samples containing perchlorate anions are electron-irradiated, CO_2 quickly leaves the parent molecule, then oxidation on the amine group of the other decarboxylation product CH_3NH_2 takes place. This consumption of CH_3NH_2 facilitates the decarboxylation being in equilibrium with the carboxylation process otherwise. This proposed mechanism is ubiquitous and also accounts for the isotopologue samples.

4.4. Destruction Rates and Carbon Dioxide Formation Rates, Mass Balances

The reduction of the vibrational bands upon irradiation was studied previously (Góbi et al. 2016a). That of one selected vibrational mode of the samples can be seen in Figure 4 and shows great similarities with our previous findings (Figures 3 and 4 in Góbi et al. 2016a). The determined decay rates (Table 4) of pure glycine samples are mostly independent of the deuterium content of the molecule and vary between 1.88×10^{-4} and $2.22 \times 10^{-4} \text{ s}^{-1}$ (they deviate from each other by no more than $\pm 10\%$), while CO_2 formation rates are between 0.22×10^{-4} and $0.29 \times 10^{-4} \text{ s}^{-1}$ (the deviation is roughly $\pm 15\%$). These findings are in good agreement with the values obtained at 10 K previously ($1.67 \times 10^{-4} \text{ s}^{-1}$ for the glycine decay rate, whereas the sum of the CO and CO_2 formation rates is $0.26 \times 10^{-4} \text{ s}^{-1}$ (Góbi et al. 2016a)). Degradation rates of parent molecules for glycine- $1\text{-}^{13}\text{C}$ - $\text{Mg}(\text{ClO}_4)_2 \cdot 6\text{H}_2\text{O}$ 5:1 and 3:1 samples ($2.67 \times 10^{-4} \text{ s}^{-1}$ and $3.13 \times 10^{-4} \text{ s}^{-1}$, respectively) are between those of the pure glycine samples (see above) and the 1:1 mixture ($3.32 \times 10^{-4} \text{ s}^{-1}$ at 10 K) used in our previous work. This can be explained by their moderate perchlorate, i.e., oxygen atom-forming, concentration as compared to the 1:1 mixture. As a consequence, their relative increases compared to the pure glycine samples (1.42 ± 0.49 and 1.66 ± 0.64 for the 5:1 and 3:1 samples) are also somewhat below that of the 1:1 mixture (2.0 ± 0.4 at 10 K). The CO_2 formation rates of the mixture samples are $(2.55 \pm 0.17) \times 10^{-4} \text{ s}^{-1}$ and $(3.06 \pm 0.20) \times 10^{-4} \text{ s}^{-1}$, which means an approximate 8–11-fold increase in CO_2 formation compared to pure glycine samples.

The mass balances were calculated as described in Góbi et al. (2016a) previously and are given in Table 5; they are in accordance with our previously presented data. The fraction of decomposed glycine is between 49% and 55% in the pure samples (compare with 57% in Table 6 of Góbi et al. 2016a). The same values are $(61 \pm 10)\%$ and $(68 \pm 9)\%$, for the 5:1 and 3:1 mixtures with $\text{Mg}(\text{ClO}_4)_2 \cdot 6\text{H}_2\text{O}$, respectively. They are thus in between the values of the pure samples and that of the 1:1 mixture (77%) used previously. The percentage of CO_2 molecules formed,

compared to the glycine decomposed, in the pure glycine samples is somewhat below 1% in all cases. This is comparable with the value of $(2.1 \pm 0.5)\%$ obtained during our previous measurements. Similarly, the same percentage values for the 5:1 and 3:1 mixtures are $(5.3 \pm 0.9)\%$ and $(12 \pm 2)\%$, which also fit with the data obtained earlier ($(11 \pm 6)\%$ for the 1:1 mixture). Determining the concentrations of other irradiation products—such as CH_3NH_2 , NH_3 , and CH_4 —from their IR intensities is less straightforward. This is a consequence of their very weak absorptions and because of their overlap with the more intense bands of the parent molecule glycine. However, an upper estimate can be given for them, which also agrees well with our previous findings. By summing up their abundances in the sample we can conclude that these molecules account for roughly 60% of the CO_2 formed, which is comparable to the approximate older value of 40% for pure zwitterionic glycine samples. The same values for the glycine- $\text{Mg}(\text{ClO}_4)_2 \cdot 6\text{H}_2\text{O}$ 5:1 and 3:1 mixtures are 14% and 6%, respectively, which are somewhat lower than the value found previously for the 1:1 mixture (30%). This could possibly also be caused by the different experimental setups used (different geometry of the IR measurements and therefore different sensitivity) and the large uncertainty in these values due to the low concentrations of these species. Nevertheless, the profound decrease in relative concentration of these products compared to CO_2 shows their efficient oxidation in the presence of perchlorate anions.

5. Conclusion and Astrophysical Implications

Our primary goal was to exploit the state-of-the-art PI-ReTOF-MS technique to uncover the decomposition and oxidation products of glycine in the presence of perchlorates, an abundant oxidizer on the Martian surface (Hecht et al. 2009; Davila et al. 2013). Pure zwitterionic glycine and glycine- $1\text{-}^{13}\text{C}$ - $\text{Mg}(\text{ClO}_4)_2 \cdot 6\text{H}_2\text{O}$ samples were exposed to energetic electrons, which simulate secondary electrons originating from the interaction of GCRs and organics in the Martian soil (Bennett et al. 2005; Bennett & Kaiser 2007). The radiolysis products were then investigated by collecting their TPD profiles (Jones & Kaiser 2013; Maity et al. 2014; Abplanalp et al. 2016). To support our data quantitatively, FTIR spectra were also collected online and in situ during the irradiation, and CASINO simulations were carried out as well. To unravel the destruction pathway and kinetics of glycine, it was also crucial to examine the radiolytic decomposition of isotope-labeled species such as glycine- $1\text{-}^{13}\text{C}$, glycine- d_5 , glycine- N,N,N-d_3 , and glycine- $2,2\text{-d}_2$.

The radiolytic decomposition of glycine and the effect of perchlorates on the destruction were studied in unprecedented detail, allowing us to deduce definite conclusions regarding the decay mechanisms. TPD profiles of the irradiated glycine, those of its fully and partially deuterated derivatives, and those of various glycine- $1\text{-}^{13}\text{C}$ - $\text{Mg}(\text{ClO}_4)_2 \cdot 6\text{H}_2\text{O}$ samples showed that the first and exclusive step is always decarboxylation (loss of CO_2 molecule). This holds true regardless of whether perchlorate anions are present or not. In pure glycine samples, the co-decarboxylation product CH_3NH_2 could also be detected by PI-ReTOF-MS along with its electron radiolysis product NH_3 . This is the very first explicit observation of these molecules upon glycine irradiation; earlier works could conclude their presence at most tentatively based on peak broadening in the FTIR spectra

(Góbi et al. 2016a). These findings have been further confirmed by the results obtained from the investigation of isotope-labeled glycine species (Table 3).

The reaction mechanism described above changes in the presence of perchlorate anions. After the decarboxylation step CH_3NH_2 is transformed (oxidized) therefore neither CH_3NH_2 nor its radiolysis product NH_3 could be detected. This (partial) oxidation of CH_3NH_2 at the nitrogen atom is facilitated by the oxygen atoms originating from the perchlorate units. These data also suggest that the oxidation of the $-\text{NH}_2$ group to $-\text{NO}_2$ seems to be faster than the decomposition of CH_3NH_2 to NH_3 followed by an oxidation to hydroxylamine (NH_2OH) or to nitrogen oxides (NO , NO_2). Although these three species all have ionization energies below 10.49 eV, they could not be detected in our studies or their concentration in the sample remains below the detection limit of our instrument. This interpretation of the results was strongly corroborated by the fact that in ^{13}C -containing glycine ($^+\text{H}_3\text{NCH}_2^{13}\text{COO}^-$) samples the formation of $^{13}\text{CO}_2$ could only be observed by excluding the possibility of alternative reactions such as the oxidation of the parent molecule glycine. The increased formation rate of CO_2 —which was already observed in many earlier works as well (see Góbi et al. 2016a and references therein)—can also be explained by the occurrence of this reaction pathway if it is considered that decarboxylation is an equilibrium process. That is, according to the Le Châtelier–Braun principle, the continuous depletion of the irradiation product CH_3NH_2 by oxidation shifts the otherwise equilibrium reaction toward the formation of the irradiation products. As a result, the elevated formation rate and accumulation of the other decarboxylation product—inert CO_2 —can be detected.

Although the decomposition of organics in the presence of oxidizers has been explored for decades, this work represents the first systematic study on the role of the Mars-relevant

species perchlorate, aiming to fully understand the decay mechanism. For the first time, the degradation products CH_3NH_2 and NH_3 were detected without any doubt in irradiated glycine samples, besides CO_2 , which is a well-known irradiation product. The explicit detection of these two species and the determination of the decomposition mechanism may have a fundamental effect on our understanding of the physicochemical fate of organic molecules on the surface of Mars. In the future, further experiments can be done to expand our knowledge of this topic by studying the reaction between CH_3NH_2 and atomic and/or molecular oxygen (O/O_2) upon electron irradiation. Investigation of alternative oxidants such as iron oxides and their effect on the organic decay is also of primary importance. Shkrob et al. (2011 and see their earlier works) found that goethite ($\alpha\text{-FeOOH}$) and hematite ($\alpha\text{-Fe}_2\text{O}_3$) can act as heterogeneous catalysts; furthermore, measurements carried out on Mars also showed that these may have a catalytic effect on the chlorination of benzene (Freissinet et al. 2015).

This work was supported by the National Aeronautics and Space Administration under Grant NNX14AG39G. M.F. acknowledges funding from the DFG under grant FO 941/1-1. The authors also would like to thank Alexandre Bergantini for his assistance during the experiments.

Appendix Infrared Absorptions and Assignments of Glycine Isotopologues

The appendix contains four Tables (6–9) listing the infrared absorptions and their assignments for the four isotope-labeled glycine samples (glycine- $1\text{-}^{13}\text{C}$, glycine- d_5 , glycine- N,N,N-d_3 , and glycine- $2,2\text{-d}_2$).

Table 6
Infrared Absorptions for the Pure Glycine- $1\text{-}^{13}\text{C}$ Isotopologue and Irradiation-induced Changes

Assignment ^{a,b}	Band Position (cm^{-1}) ^c		Signal Strength ^d	Change Upon Irradiation ^e
	Before Irradiation	After Irradiation		
$\delta_{\text{as}} \text{NH}_3^+ \times 2^f$				
$\nu_{\text{as}}^{13}\text{COO}^- \times 2^f$	3325.9sh, 3290.0	3325.9sh, 3286.8	w	–
$\nu_{\text{s}} \text{NH}_3^+ \times 2^f$				
$\nu_{\text{as}} \text{NH}_3^+$	3185.2, 3125.7w, 3085.1sh, 3063.2w	3180.5, 3125.7sh, 3085.1sh, 3061.6w	s	–, b
$\nu_{\text{as}} \text{CH}_2$	3006.9	3006.9sh	w	–
$\nu_{\text{s}} \text{CH}_2$	2975.6, 2964.4	2980.3, 2964.7	w	–, b
$\nu_{\text{s}} \text{NH}_3^{+g}$	2892.7, 2884.9, 2869.3sh, 2813.0	2892.7, 2886.5sh, 2858.3, 2816.1	s, b	–, b
$\nu_{\text{s}} \text{NH}_3^{+g}$	2759.8, 2733.2	2759.8, 2737.9sh	s, b	–, b
$\nu_{\text{s}} \text{NH}_3^{+g}$	2656.6sh, 2608.1, 2589.3sh	2647.2sh, 2614.3	s, b	–, b
$\nu_{\text{s}} \text{NH}_3^{+g}$	2551.8, 2528.3	2556.5, 2525.2	sh, b	–, b
$\nu_{\text{s}} \text{NH}_3^{+g}$	2465.8, 2454.8	2457.2	sh	–
$\nu_{\text{as}}^{13}\text{CO}_2^h$	–	2278.1sh	w	+
$\nu_{\text{as}}^{13}\text{COO}^- + \omega^{13}\text{COO}^-^i$	2282.8, 2215.6	2282.8, 2215.6	w	–
$\delta_{\text{as}} \text{NH}_3^+ + \tau \text{CN}^i$	2187.4, 2165.5, 2126.4, 2099.8	2184.2sh, 2167.1, 2131.1, 2099.8sh	w, b	–
$\delta_{\text{s}} \text{NH}_3^+ + \delta \text{NC}^{13}\text{C}^i$	1830.8	–	vw	–
$\delta_{\text{as}} \text{NH}_3^+$	1683.8, 1666.6	1685.4sh, 1666.6	m	–, b
$\delta_{\text{as}} \text{NH}_3^+$	1636.9, 1616.6	1636.9, 1616.6	sh	–, b
$\nu_{\text{as}}^{13}\text{COO}^-$	1574.3	1574.3	s	–, b
$\delta_{\text{s}} \text{NH}_3^+$	1546.1, 1499.3, 1486.8	1544.6, 1496.1, 1485.2	s	–, b
δCH_2	1446.1, 1439.8sh	1446.1, 1439.8sh	s	–, b
$\nu_{\text{s}}^{13}\text{COO}^-$	1410.1, 1394.4sh	1410.1, 1394.4sh	s	–, b
ωCH_2	1328.8	1328.8	m	–, b

Table 6
(Continued)

Assignment ^{a,b}	Band Position (cm ⁻¹) ^c		Signal Strength ^d	Change Upon Irradiation ^e
	Before Irradiation	After Irradiation		
tw CH ₂	1306.9	1306.9	w	-, b
ρ NH ₃ ⁺	1138.0	1138.0	m	-
ρ NH ₃ ⁺	1112.9	1112.9	m	-
ν CN	1044.1	1044.1	m	-
ρ CH ₂	908.1	908.1	m	-
ν C ¹³ C	890.8	890.8	m	-
δ ¹³ COO ⁻	703.2	703.2	m	-, b

Notes.

^a Assignments based on previous experimental studies (see references in text). For those of the glycine and glycine-Mg(ClO₄)₂ · 6H₂O mixtures see Góbi et al. (2016a).

^b ν : stretching, δ : bending, ω : wagging, tw: twisting, ρ : rocking, τ : torsional, s: symmetric, as: antisymmetric vibrations.

^c -: no signal, sh: shoulder, w: weak band.

^d s: strong, m: medium, (v)w: (very) weak, sh (shoulder), (v)b: (very) broad band.

^e -: band decreases, +: band increases, b: broadening upon irradiation.

^f Overtone, tentative assignment.

^g Fermi resonance, for tentative assignment see Rosado et al. (1998).

^h Stretching vibration of irradiation product ¹³CO₂ it overlaps with ν_{as} ¹³COO⁻ + ω ¹³COO⁻¹.

ⁱ Combinational band, tentative assignment. $\nu(\delta$ NCC) = 358 cm⁻¹ (Furić et al. 1992).

Table 7
Infrared Absorptions for the Pure Glycine-d₅ Isotopologue and Irradiation-induced Changes

Assignment ^{a,b}	Band Position (cm ⁻¹) ^c		Signal Strength ^d	Change Upon Irradiation ^e
	Before Irradiation	After Irradiation		
ν_{as} ND ₃ ⁺	2390.7, 2345.3, 2339.1	2390.7, 2345.3, 2339.1	s	-, b
ν_{as} CO ₂ ^f	-	-	-	N/A
ν_{as} CD ₂	2262.4	2262.4	m	-, b
ν_s CD ₂	2220.2, 2209.3sh	2221.8, 2209.3sh	m	-, b
ν_s ND ₃ ^{+g}	2176.4, 2149.8, 2140.5, 2127.9sh	2176.4, 2146.7sh, 2138.9, 2127.9sh	s, b	-, b
ν_s ND ₃ ^{+g}	2062.3	2065.4	s, b	-, b
ν_s ND ₃ ^{+g}	1996.6	1996.6	s, b	-, b
ν_s ND ₃ ^{+g}	1910.6	1910.6	sh	-, b
δ_{as} ND ₃ ⁺ + τ CN ^h	1837.0, 1791.7, 1771.4	1837.0, 1791.7, 1774.5	w, b	-
δ_s ND ₃ ⁺ + δ NCC ^h	1738.5sh, 1730.7	1738.5sh, 1730.7	vw	-
ν_{as} COO ⁻	1558.7, 1532.1, 1518.0sh	1558.7, 1528.9sh, 1518.0sh	s	-, b
ν_s COO ⁻	1433.5, 1413.2, 1396.0, 1375.7	1432.0sh, 1413.2, 1394.4, 1377.2	s	-, b
δ_{as} ND ₃ ⁺	1255.3	1255.3	w	-
δ_s ND ₃ ⁺ , δ CD ₂	1177.1sh, 1169.2, 1148.9, 1139.5	1525.6sh, 1512.5, 1497.8sh	s	-
ν CN	1084.8, 1076.9, 1058.2	1084.8sh, 1076.9, 1058.2	m	-
ω CD ₂ , tw CD ₂	922.1, 897.1	922.1, 897.1	m	-, b
ν CC	872.1	872.1	m	-
ρ CD ₂ , ρ ND ₃ ⁺	958.1, 806.4, 792.3, 751.7, 739.1	958.1, 806.4, 792.3, 751.7, 739.1	m	-
δ COO ⁻	709.4	709.4	m	-

Notes.

^a Assignments based on previous experimental studies (see references in text). For those of the glycine and glycine-Mg(ClO₄)₂ · 6H₂O mixtures see Góbi et al. (2016a).

^b ν : stretching, δ : bending, ω : wagging, tw: twisting, ρ : rocking, τ : torsional, s: symmetric, as: antisymmetric vibrations.

^c -: no signal, sh: shoulder, w: weak band.

^d s: strong, m: medium, (v)w: (very) weak, sh (shoulder), (v)b: (very) broad band.

^e -: band decreases, +: band increases, b: broadening upon irradiation, N/A: not observable.

^f Stretching vibration of irradiation product CO₂, indistinguishable from ν_{as} ND₃⁺.

^g Fermi resonance, for tentative assignment see Rosado et al. (1998).

^h Combinational band, tentative assignment. $\nu(\delta$ NCC) = 358 cm⁻¹ (Furić et al. 1992).

Table 8
Infrared Absorptions for the Pure Glycine-N,N,N-d₃ Isotopologue and Irradiation-induced Changes

Assignment ^{a,b}	Band Position (cm ⁻¹) ^c		Signal Strength ^d	Change Upon Irradiation ^e
	Before Irradiation	After Irradiation		
$\nu_{\text{as}} \text{CH}_2$	3006.9	3006.9sh	m	-, b
$\nu_{\text{s}} \text{CH}_2$	2972.5, 2963.1	2972.5, 2963.1	m	-, b
$\nu_{\text{as}} \text{ND}_3^+$	2396.9, 2384.4, 2342.2, 2292.2	2396.9, 2384.4, 2342.2, 2292.2	s, b	-, b
$\nu_{\text{as}} \text{CO}_2^{\text{f}}$	–	–	–	N/A
$\nu_{\text{s}} \text{ND}_3^{+\text{g}}$	2260.9, 2243.7, 2203.0, 2182.7, 2145.1	2260.9, 2243.7, 2203.0, 2182.7, 2145.1	s, b	-, b
$\nu_{\text{s}} \text{ND}_3^{+\text{g}}$	2066.9, 2009.1	2759.8, 2737.9sh	s, b	-, b
$\nu_{\text{s}} \text{ND}_3^{+\text{g}}$	1938.7, 1858.9	1938.7, 1858.9	sh	-, b
$\nu_{\text{as}} \text{COO}^-$	1564.9, 1538.3, 1491.4	1564.9, 1538.3, 1491.4	s	-, b
δCH_2	1446.1	1446.1	w	–
$\nu_{\text{s}} \text{COO}^-$	1430.4, 1425.7, 1419.5, 1405.4	1430.4, 1425.7, 1419.5, 1405.4	s	-, b
$\omega \text{CH}_2, \text{tw} \text{CH}_2$	1319.4	1319.4	m	-, b
$\delta_{\text{as}} \text{ND}_3^+$	1267.8, 1219.3	1267.8, 1219.3	m	-, b
$\delta_{\text{s}} \text{ND}_3^+$	1180.2, 1170.8, 1161.4	1180.2, 1169.2, 1161.4sh	s	-, b
νCN	1042.6, 1031.7	1042.6, 1031.7	m	–
ρCH_2	967.5	908.1	w	–
νCC	887.7	887.7	w	–
ρND_3	825.2, 792.3, 770.4, 767.3, 754.8	825.2, 792.3, 770.4sh, 767.3, 754.8	m	–
δCOO^-	684.4	684.4	m	–

Notes.

^a Assignments based on previous experimental studies (see references in text). For those of the glycine and glycine–Mg(ClO₄)₂ · 6H₂O mixtures see Góbi et al. (2016a).

^b ν : stretching, δ : bending, ω : wagging, tw: twisting, ρ : rocking, τ : torsional, s: symmetric, as: antisymmetric vibrations.

^c –: no signal, sh: shoulder, w: weak band.

^d s: strong, m: medium, (v)w: (very) weak, sh (shoulder), (v)b: (very) broad band.

^e –: band decreases, +: band increases, b: broadening upon irradiation, N/A: not observable.

^f Stretching vibration of irradiation product CO₂, indistinguishable from $\nu_{\text{as}} \text{ND}_3^+$.

^g Fermi resonance, for tentative assignment see Rosado et al. (1998).

Table 9
Infrared Absorptions for the Pure Glycine-2,2-d₂ Isotopologue and Irradiation-induced Changes

Assignment ^{a,b}	Band Position (cm ⁻¹) ^c		Signal Strength ^d	Change Upon Irradiation ^e
	Before Irradiation	After Irradiation		
$\delta_{\text{as}} \text{NH}_3^+ \times 2^{\text{f}}$				
$\nu_{\text{as}} \text{COO}^- \times 2^{\text{f}}$	3318.1sh, 3283.7	3318.1sh, 3283.7	w	–
$\nu_{\text{s}} \text{NH}_3^+ \times 2^{\text{f}}$				
$\nu_{\text{as}} \text{NH}_3^+$	3200.8, 3177.7, 3071.0	3199.3, 3177.7, 3071.0	s	-, b
$\nu_{\text{s}} \text{NH}_3^{+\text{g}}$	2916.2, 2844.2, 2806.4	2916.2, 2844.2, 2806.4	s, b	-, b
$\nu_{\text{s}} \text{NH}_3^{+\text{g}}$	2759.8, 2733.2	2759.8, 2737.9sh	s, b	-, b
$\nu_{\text{s}} \text{NH}_3^{+\text{g}}$	2764.5sh, 2701.9, 2673.8, 2630.0	2764.5sh, 2700.4, 2675.3, 2630.0	s, b	-, b
$\nu_{\text{s}} \text{NH}_3^{+\text{f}}$	2575.2, 2564.3, 2443.9	2575.2, 2564.3, 2443.9	sh, b	-, b
$\nu_{\text{as}} \text{CO}_2^{\text{h}}$	–	2342.2sh	sh	+
$\nu_{\text{as}} \text{CD}_2$	2256.2	2256.2	w	–
$\nu_{\text{s}} \text{CD}_2$	2162.3sh, 2159.2	2162.3sh, 2159.2	m	-, b
$\nu_{\text{as}} \text{COO}^- + \omega \text{COO}^{-\text{i}}$	2234.3	2234.3	w	–
$\delta_{\text{as}} \text{NH}_3^+ + \tau \text{CN}^{\text{f}}$	2187.4, 2135.8, 2118.6, 2092.0	2187.4sh, 2135.8sh, 2118.6, 2092.0	w	–
$\delta_{\text{s}} \text{NH}_3^+ + \delta \text{NCC}^{\text{i}}$	1852.7	1852.7	vw	–
$\delta_{\text{as}} \text{NH}_3^+$	1665.0	1665.0	m	-, b
$\delta_{\text{s}} \text{NH}_3^+$	1633.7, 1621.2	1633.7, 1621.2	s	-, b
$\nu_{\text{as}} \text{COO}^-$	1593.1, 1566.5sh	1593.1, 1566.5sh	s	-, b
$\delta_{\text{s}} \text{NH}_3^+$	1544.6, 1519.6, 1499.2, 1474.2sh	1544.6, 1519.6, 1497.7, 1474.2sh	s	-, b
$\nu_{\text{s}} \text{COO}^-$	1433.5, 1411.7sh	1433.5, 1411.7sh	s	-, b
$\nu_{\text{s}} \text{COO}^-$	1410.1, 1394.4sh	1410.1, 1394.4sh	s	-, b
$\delta \text{CD}_2, \rho \text{NH}_3^+$	1211.5, 1194.3, 1169.2, 1114.5	1211.5, 1194.3, 1169.2, 1114.5	s	-, b
νCN	1059.8, 1048.8	1059.8, 1048.8	m	–
$\omega \text{CD}_2, \text{tw} \text{CD}_2$	928.4, 919.0, 911.2sh	928.4, 919.0, 911.2sh	m	-, b

Table 9
(Continued)

Assignment ^{a,b}	Band Position (cm ⁻¹) ^c		Signal Strength ^d	Change Upon Irradiation ^e
	Before Irradiation	After Irradiation		
ν CC	872.1, 842.4sh	872.1, 842.4sh	m	–
ρ CD ₂	801.7	801.7	m	–
δ COO ⁻	679.7	679.7	m	–, b

Notes.

^a Assignments based on previous experimental studies (see references in text). For those of the glycine and glycine–Mg(ClO₄)₂ · 6H₂O mixtures see Góbi et al. (2016a).

^b ν : stretching, δ : bending, ω : wagging, tw: twisting, ρ : rocking, τ : torsional, s: symmetric, as: antisymmetric vibrations.

^c –: no signal, sh: shoulder, w: weak band.

^d s: strong, m: medium, (v)w: (very) weak, sh (shoulder), (v)b: (very) broad band.

^e –: band decreases, +: band increases, b: broadening upon irradiation, N/A: not observable.

^f Overtone, tentative assignment.

^g Fermi resonance, for tentative assignment see Rosado et al. (1998).

^h Stretching vibration of irradiation product ¹³CO₂.

ⁱ Combinational band, tentative assignment. $\nu(\delta$ NCC) = 358 cm⁻¹ (Furić et al. 1992).

References

- Abplanalp, M. J., Förstel, M., & Kaiser, R. I. 2016, *CPL*, 644, 79
- Acuña, M. H., Connerney, J. E. P., Ness, N. F., et al. 1999, *Sci*, 284, 790
- Armstrong, J. C., Leovy, C. B., & Quinn, T. 2004, *Icar*, 171, 255
- Aue, D. H., Webb, H. M., & Bowers, M. T. 1976, *JChS*, 98, 311
- Barlow, S. M., Kitching, K. J., Haq, S., & Richardson, N. V. 1998, *SurSc*, 401, 322
- Bazsó, G., Magyarfalvi, G., & Tarczay, G. 2012, *JMoSt*, 1025, 33
- Bennett, C. J., Jamieson, C. S., Osamura, Y., & Kaiser, R. I. 2005, *ApJ*, 624, 1097
- Bennett, C. J., & Kaiser, R. I. 2007, *ApJ*, 660, 1289
- Berkowitz, J., Greene, J. P., Cho, H., & Ruscic, B. 1987, *JChPh*, 86, 674
- Biemann, K., & Bada, J. L. 2011, *JGRE*, 116, E12001
- Biemann, K., Oró, J., Toulmin, P., et al. 1976, *Sci*, 194, 72
- Botta, O., & Bada, J. L. 2002, *SGeo*, 23, 411
- Cannington, P. H., & Ham, N. S. 1983, *JESRP*, 32, 139
- Carrier, B. L., & Kounaves, S. P. 2015, *GeoRL*, 42, 3739
- Chevrier, V. F., Hanley, J., & Altheide, T. S. 2009, *GeoRL*, 36, L10202
- Cockell, C. S., & Raven, J. A. 2004, *Icar*, 169, 300
- Collin, J. E., & Franskin, M. J. 1966, *BSRSL*, 35, 267
- Coppens, P., Smets, J., Fishel, M. G., & Drowart, J. 1974, *IJMP*, 14, 57
- Dartnell, L. R., Desorgher, L., Ward, J. M., & Coates, A. J. 2007, *GeoRL*, 34, L02207
- Davila, A. F., Willson, D., Coates, J. D., & McKay, C. P. 2013, *IJAsB*, 12, 321
- Dibeler, V. H., Walker, J. A., & Liston, S. K. 1967, *JRNBA*, 71, 371
- Drouin, D., Couture, A. R., Joly, D., et al. 2007, *Scanning*, 29, 92
- Ebata, T., Anezaki, Y., Fujii, M., Mikami, N., & Ito, N. 1983, *JPhCh*, 87, 4773N
- Encrenaz, T., Bézard, B., Greathouse, M. J., et al. 2004, *Icar*, 170, 424
- Encrenaz, T., Greathouse, T. K., Lefevre, F., & Atreya, S. K. 2012, *P&SS*, 68, 3
- Fethi, F., López-Gejo, J., Köhler, M., & Braun, A. M. 2008, *Journal of Advanced Oxidation Technologies*, 11, 208
- Flynn, G. J. 1996, *EM&P*, 72, 469
- Freissinet, C., Glavin, D. P., Mahaffy, P. R., et al. 2015, *JGRE*, 120, 495
- Furić, K., Mohaček, V., Bonifačić, M., & Štefanić, I. 1992, *JMoSt*, 267, 39
- García, G. A., Gans, B., & Tang, X. 2015, *JESRP*, 203, 25
- Gerakines, P. A., & Hudson, R. L. 2015, *Icar*, 252, 466
- Gerakines, P. A., Hudson, R. L., Moore, M. H., & Bell, J.-L. 2012, *Icar*, 220, 647
- Glavin, D. P., Freissinet, C., Miller, K. E., et al. 2013, *JGRE*, 118, 1955
- Góbi, S., Abplanalp, M. J., & Kaiser, R. I. 2016a, *ApJ*, 822, 8
- Góbi, S., Bergantini, A., & Kaiser, R. I. 2016b, *ApJ*, 832, 164
- Grenie, Y., & Garrigou-Lagrange, C. 1972, *JMoSt*, 41, 240
- Hassler, D. M., Zeitlin, C., Wimmer-Schweingruber, R. F., et al. 2014, *Sci*, 343, 1244797
- Hecht, M. H., Kounaves, S. P., Quinn, R. C., et al. 2009, *Sci*, 325, 64
- Herranz, J., & Delgado, J. M. 1975, *AcSpA*, 31, 1245
- Hilbig, R., & Wallenstein, R. 1981, *IJQE*, 17, 1566
- Holtom, P. D., Bennett, C. J., Osamura, Y., Mason, N. J., & Kaiser, R. I. 2005, *ApJ*, 626, 940
- Houck, R. C. 1930, *JChS*, 52, 2420
- Jackson, W. A., Davila, A. F., Sears, D. W. G., et al. 2015, *E&PSL*, 430, 470
- Jochims, H.-W., Schwell, M., Chotin, J.-L., et al. 2004, *CP*, 298, 279
- Jones, B. M., & Kaiser, R. I. 2013, *JPCL*, 4, 1965
- Kim, Y. S., Wo, K. P., Maity, S., Atreya, S. K., & Kaiser, R. I. 2013, *JChS*, 135, 4910
- Kminek, G., & Bada, J. L. 2006, *E&PSL*, 245, 1
- Leshin, L. A., Mahaffy, P. R., Webster, C. R., et al. 2013, *Sci*, 341, 1238937
- Lewis, R. J., Sr. (ed.) 2007, *Hawley's Condensed Chemical Dictionary* (15th ed.; Hoboken, NJ: Wiley), 779
- Litorja, M., & Ruscic, B. 1998, *JChPh*, 108, 6748
- Locht, R., Hottmann, K., Hagenow, G., Denzer, W., & Baumgärtel, H. 1992, *CPL*, 190, 124
- Lossing, F. P., Lam, Y.-T., & Maccoll, A. 1981, *CaJCh*, 59, 2228
- Maity, S., Kaiser, R. I., & Jones, B. M. 2014, *FaDi*, 168, 485
- Maté, B., Tanarro, I., Escribano, R., Moreno, M. A., & Herrero, V. J. 2015, *ApJ*, 806, 151
- Maté, B., Tanarro, I., Moreno, M. A., et al. 2014, *FaDi*, 168, 267
- McCurry, D. L., Quay, A. N., & Mitch, W. A. 2016, *EnST*, 50, 1209
- Melton, C. E. 1966, *JChPh*, 45, 4414
- Miller, K. E., Eigenbrode, J. L., Freissinet, C., et al. 2016, *JGRE*, 121, 296
- Molina-Cuberos, G. J., Stumptner, W., Lammer, H., Kömle, N. I., & O'Brien, K. 2001, *Icar*, 154, 216
- Moore, J. E., & Schuerger, A. C. 2012, *JGRE*, 117, E08008
- Muñoz-Caro, G. M., Mateo-Martí, E., & Martínez-Frías, J. 2006, *Sensors*, 6, 688
- Oró, J., & Holzer, G. 1979, *JMoE*, 14, 153
- Parr, G. R., & Taylor, J. W. 1974, *IJMP*, 14, 467
- Pavlov, A. A., Vasilyev, G., Ostryakov, V. M., Pavlov, A. K., & Mahaffy, P. 2012, *GeoRL*, 39, L13202
- Pilling, S., Mendes, L. A. V., Bordalo, V., et al. 2013, *AsBiol*, 13, 79
- Pilling, S., Nair, B. G., Escobar, A., Fraser, H., & Mason, N. 2014, *EPJD*, 68, 58
- Rosado, M. T., Duarte, M. L. T., & Fausto, R. 1998, *VibSpectr*, 16, 35
- Shkrob, I. A., Marin, T. M., Chemerisov, S. D., & Sevilla, M. D. 2011, *JPCC*, 115, 4642
- Smith, M. L., Claire, M. W., Catling, D. C., & Zahnle, K. J. 2014, *Icar*, 231, 51
- Stoker, C. R., & Bullock, M. A. 1997, *JGRE*, 102, 10881
- Sutter, B., Ming, D. W., Boynton, W. V., et al. 2009, *LPICo*, 1502, 29
- Suzuki, S., Shimanouchi, T., & Tsuboi, M. 1963, *AcSpe*, 19, 1195
- ten Kate, I. L. 2010, *AsBiol*, 10, 589
- ten Kate, I. L., Garry, J. R. C., Peeters, Z., et al. 2005, *M&PS*, 40, 1185
- Toner, J., Catling, D., & Light, B. 2014, *GeCoA*, 136, 142
- Tsegaw, Y. A., Sander, W., & Kaiser, R. I. 2016, *JPCA*, 120, 1577
- Turner, A. M., Abplanalp, M. J., & Kaiser, R. I. 2016, *ApJ*, 820, 127
- VonDrasek, W. A., Okajima, S., & Hessler, J. P. 1988, *ApOpt*, 27, 4057
- Watanabe, K., Nakayama, T., & Motil, J. 1962, *JQSRT*, 2, 369
- Webber, W. R., & Lezniak, J. A. 1974, *Ap&SS*, 30, 361
- Wilson, E. H., Atreya, S. K., Kaiser, R. I., & Mahaffy, P. R. 2016, *JGRE*, 121, 1472
- Yang, B., Wang, J., Cool, T. A., et al. 2012, *IJMSp*, 309, 118
- Zaretskii, V. I., Sadovskaya, V. L., Wulfson, N. S., Sizoy, V. F., & Merimson, V. G. 1971, *OrMSp*, 5, 1179